ABSTRACT

CHEN, JIYANG. A Biodegradable Knitted Cardiac Patch For Myocardium Regeneration Using Cardiosphere-derived Cells (CDCs) (Under the direction of Marin W. King.)

Based on the statistics of the latest heart disease study, an American will die of cardiovascular disease (CVD) every few seconds. In recent years, more patients have been able to survive an acute myocardial infarction (MI) (or heart attack) caused by CVD, but the recovery of the damaged myocardium is still a challenge. The use of tissue engineering therapies can regenerate myocardial tissue at the site of injury by delivering stem cells directly to the surface of the scar site. An injection method is commonly used to directly deliver the cells, but the survival rate of the cells is extremely low. As an alternative to a direct injection strategy, the use of a cardiac patch can prevent the cells from being dispersed and it can also support the cell delivery process by promoting cell attachment and proliferation. In addition, the cardiac patch can provide mechanical support to the ventricular wall while it experiences the remodeling process. Today there are a number of different kinds of cardiac patches that have been developed to assist in the recovery of the defective function of the left ventricle. But the remaining question that has not been answered is how to design a cardiac patch that can mimic the non-linear mechanical properties of human myocardium. In an attempt to answer this question the present study proposes that weft knitted fabrics can match the compliance and recovery of myocardium. Another critical requirement for the successful design of a tissue engineered cardiac patch is the selection of the appropriate cell line. In this study cardiosphere derived stem cells (CDCs) were used, as they are known to have the potential to differentiate into various kinds of tissue. For example, from previous research studies when CDCs were injected directly into a rat model, the function of the left ventricles improved significantly. In this study, various prototype textile structures were weft

knitted from polyester (polyethylene terephthalate) (PET) yarns in a preliminary step, and their thickness, mass per unit area and mechanical properties were measured. The initial tensile modulus of a tuck stitch structure was similar to that of human myocardium. The rib stitch structure had the highest total porosity, while the jersey stitch structure had the lowest. So based on the results from the stretch and recovery test and the calculated total porosity, these three particular weft knitted structures, with jersey, tuck and rib stitches were selected as candidates for further evaluation as a cardiac patch knitted from polylactic acid (PLA) yarns. In subsequent uniaxial and biaxial stress tests, the tuck stitch structure gave a similar stress-strain curve and Young's modulus to that of human myocardium. In contrast, the jersey stitch sample had much higher stiffness than human myocardium. From the biological cell culture *in vitro* tests, scanning electron microscopy (SEM) confirmed the attachment and proliferation of CDCs on the surface of the PLA fibers. And the results of an MTT proliferation assay showed that the rib stitch sample produced a significantly higher yield of cells than the other two samples. In conclusion, the rib stitch structure was found to be the most promising choice for the design of a PLA knitted cardiac patch. Further animal studies will be needed in order to demonstrate that a textile cardiac patch weft knitted from PLA yarns can function successfully *in vivo*.

A Biodegradable Knitted Cardiac Patch For Myocardium Regeneration Using Cardiosphere-derived Cells (CDCs)

by
Jiyang Chen

A thesis submitted to the Graduate Faculty of
North Carolina State University
in partial fulfillment of the
requirements for the degree of
Master of Science

Textile Engineering

Raleigh, North Carolina

2015

APPROVED BY:

_____	_____
Dr. Martin W. King Committee Chair	Dr. Andre J. West
_____	
Dr. Ke Cheng	

DEDICATION

To my beloved family.

BIOGRAPHY

Jiyang Chen was born on October 4th, 1991 China. He received his bachelor's degree. in Textile Engineering in July 2013 from Donghua University, Shanghai, P.R. China. In order to pursue further studies, he was accepted into an exchange program between Donghua University and North Carolina State University in 2012.He joined in Dr King's biomedical textile research group and continued his study of biomedical textile devices. He is expected to receive his master degree in August 2015, and plans to continue his study for a doctoral degree in the College of Textiles at NCSU.

ACKNOWLEDGMENTS

First of all, I appreciate College of Textiles, North Carolina State University for offering me a great opportunity to do further research in biomedical textiles. During the last two years, I have learnt about the practical writing skills and experimental laboratory techniques.

I wish to express my sincere thanks to Dr. Martin W. King who is an expert in biomedical textiles and biomaterials. He provided me with the chance to do this study. Thanks to his support, I have become familiar with advanced knowledge and experimental skills that I will need in my further research. Moreover, his passion for work and life inspires me and all the students in his group.

I also appreciate the support given by the other members of my Advisory Committee, Dr. Andre Julian West and Dr. Ke Cheng. They helped me to knit all the samples and provided the cells and supplies I needed for this study. They also offered valuable suggestions about different aspects for my written thesis.

There are many other people who helped me during this research. I would like to convey my gratitude to Ting He, Taylor Hensley, Bryan Danley, Dr Hsiao-Ying Huang, Hui Cong and Yu Xie for advising me about laboratory skills and experimental methods. When I met troubles in my experiments, they offered me their personal experience and suggestions. In particular, Ting He taught me about the use of specific laboratory procedures to be followed and cautioned me about potential hazards to be avoided during cell culture experiments which saved me a lot of time.

Last but not least, I would like to express my deep appreciation to my family in China. They have always supported me, encouraged me and inspired me.

TABLE OF CONTENTS

LIST OF TABLES

LIST OF FIGURES

CHAPTER 1

GENERAL INTRODUCTION

1.1 Background and Motivation

Based on the latest epidemiological statistics, death caused by cardiovascular disease (CVD) accounted for 31.9% of all deaths in the US in 2010. Coronary heart disease (CHD) alone caused approximately 1 in every 6 deaths in the US in 2010. Every 1 minute 23 seconds, an American would die of an adverse coronary event. Although the mortality attributed to CVD declined 31.0% from the year 2000 to 2010 due to the investment of hundreds of billions of dollars every year, over 2150 Americans die of CVD each day (Go et al., 2014) Although many patients can survive an acute heart attack, apoptosis (or cell death) of cardiomyocytes is unavoidable, which means that the cardiac function for such patients is decreased by 20-40% (Cheng et al., 2012). As a result, the heart needs to be remodeled so as to ensure that there is sufficient blood supply to metabolize all organs and tissues. Otherwise the patient is at risk of another infarction and major heart failure. According to a recent report, mortality due to heart failure is approximately as high as it was in 1995, which means that the recovery of cardiac function following a heart attack has not improved over the last 20 years. For these initial-stage heart failure patients, a cardiac patch would be useful for regenerating cardiomyocytes. While for patients presenting with end-stage heart failure, their highly morbid condition will always limit their treatment options. (Sale et al., 2012)

1.2 Objectives

The overall goal of this study was to fabricate and evaluate a textile heart patch knitted from polylactic acid (PLA) yarns, which is able to support the growth of cardiosphere-derived stem cells (CDCs). Prior to reaching this goal, a series of knitted prototype structures was fabricated from polyester yarns and their mechanical properties determined in order to find which sample closely mimicked the mechanical stiffness of cardiac muscle. Then, after the selected "candidate structures" had been knitted from PLA yarns, their biological performance was determined by a CDC in vitro culture assay so as to observe their attachment, growth and proliferation.

The five specific objectives for the study are listed below. They describe how the overall aim of the study has been accomplished including the necessary mechanical evaluations and biological observations.

1. To initially fabricate a series of polyester prototype samples with different weft knitted structures and design including jersey, tuck, pointelle, twill, rib and miss stitches. In addition, samples were knitted from 3-ply folded yarns consisting of two ends of polyester and one end of spandex yarn with the same stitch structures so as to observe any change in mechanical properties due to the addition of spandex. The porosity, thickness, mass per unit area and stitch density of the samples were measured so as to provide a base line for selecting the "candidate" PLA knitted structures.

2. To evaluate the initial modulus of the polyester samples using a uniaxial Instron tensile machine to establish which stitch structures mimicked most closely the mechanical properties of human cardiac tissue.

3. To fabricate the selected "candidate" structures weft knitted from PLA yarns and to evaluate their mechanical properties by both a uniaxial Instron machine and a biaxial tensile tester.

5. To determine the influence of porosity, stitch type and stitch count on the attachment, growth and proliferation of the CDCs.

1.3 Significance

In this study, there are two significant points that are worth mentioning. First, while there is a range of different techniques for the delivery of cells to the cardiac site of interest, the survival rate of the cells delivered, for example by injectable platelet gel, is extremely low, and the gel will degrade in 14 days (Miyagi, Y et al 2011.) The second point relates to the rigidity or lack of compliance associated with current tissue engineering scaffolds or cardiac patches fabricated from synthetic polymer foams, gels and membranes. In order to achieve 20% strain, the current cardiac patch materials can experience mechanical stresses as high as 1-10 MPa (Prabhakaran et al., 2011), which is significantly higher than that of human cardiac tissue (5-7 KPa). (Chen et al., 2008). As a result such rigid patch materials can compromise diastole and the ability of the heart to relax. The unique features of weft knitted fabrics are their low initial modulus, flexibility and high porosity, which means that such knitted patches can have similar mechanical compliance to cardiac muscle. However, previous studies have

reported using polyester and expanded polytetrafluoroethylene (ePTFE) materials for knitting heart patch scaffolds. These two materials have significant risks such as a loss in mechanical properties over time, inducing infection, and limiting the ability of the tissue to remodel. (Pok, S. et al 2011)(Mirensky, T. et al, 2008). In comparison, PLA has both superior biocompatibility and appropriate mechanical performance. In summary, it is believed that the novel three dimensional scaffold or cardiac patch knitted from PLA yarns can provide a mechanical performance similar to cardiac tissue as well as supporting the attachment and proliferation of CDC stem cells.

CHAPTER 2

LITERATURE REVIEW

2.1 Pathology of Heart Failure

2.1.1 Causes of Heart Failure

Heart failure (HF) usually means chronic heart failure (CHF), which can be defined as insufficient cardiac output to meet the needs of the body.

The cause of CHF is a culmination of cardiac muscle pathophysiology from diverse etiologies including ischemic heart disease, auto-immune infections, extrinsic force etc (Raman, J. 2008), which can be any condition that limits cardiomyocyte survival. Functional cardiomyocyte loss would be caused by various conditions including myocardial infarction (MI), high blood pressure (HBP) and other kind of cardiovascular disease (CVD).

Myocardial infarction will now be taken as an example for explaining the cause of heart failure in more detail. Due to atherosclerosis, an unhealthy diet, lack of activity and smoking (Go et al., 2014), the compliance of arteries decreases which contributes to a lower rate of blood flow. This leads to certain lipids in the blood, such as cholesterol, to precipitate on the inner wall of arteries and cause them to narrow (stenose) and eventually become blocked (occluded). Acute myocardial infarction (AMI) occurs when a coronary artery is blocked due to lipid deposits (plaque) or a superimposed thrombus. (Arnal-Pastor et al., 2013) Once a coronary artery is blocked, the downstream zone experiences a lack of oxygen, nutrients and

metabolites. A decrease in the pH value and a reduction in the contractile function caused by anaerobic glycolysis follows (Burke et al., 2010). The zone where myocytes remain viable may reduce the metabolism and the oxygen consumption necessary to survive.

In cardiac surgery, the main goal is to limit the severity and extent of AMI. The most common therapy is reperfusion that can restore blood flow inside the heart and a rapid supply of nutrients and oxygen to myocardial tissues. This is able to alleviate the ischemia. However, reperfusion changes the microenvironment of the heart by inducing apoptosis because of toxic substances released during reperfusion. After AMI, cardiomyocytes and tissues are injured, and a compensatory mechanism is activated to recover the cardiac function.

2.1.2 Remodeling after Acute Myocardial Infarction

Compensatory mechanisms and the progressive model of the post-MI stage are very complex. So we are focusing on remodeling due to the loss of the left ventricular cardiomyocytes.

The most common causes of ventricle remodeling are hypertensive heart disease (HHD) and ischemic heart disease associated with prior myocardial infarction, that are also known as post-MI remodeling.

For HHD remodeling, the feature of that is a normal-sized chamber and preserved systolic function with left ventricular (LV) hypertrophy. Once the left ventricular ejection fraction (LVEF) is greater than 50%, patients with heart failure begin to experience symptoms, and their left ventricle hypertrophy (LVH) can lead to heart failure in a comparatively short time.

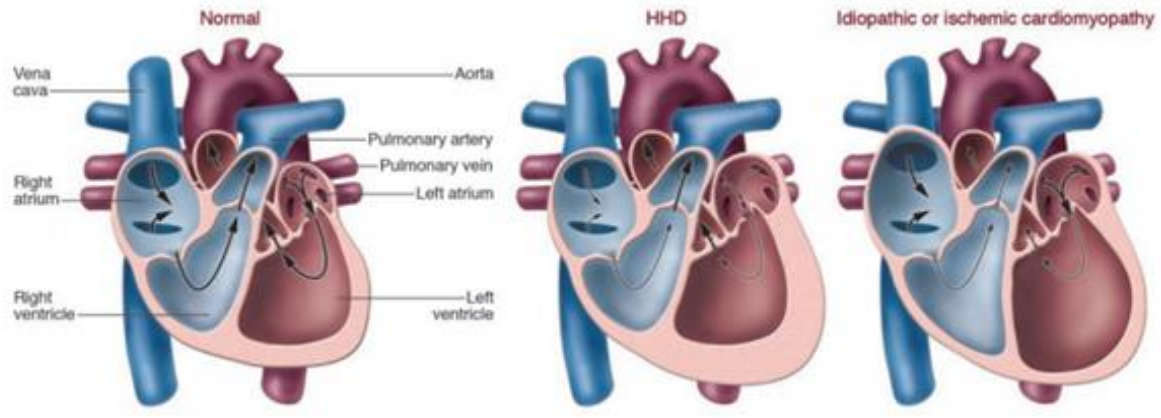

Fig 2.1 Changes in the cardiac chambers caused by HHD and ischemic cardiomyopathy

(Copyright: Bradford C. Berk, 2007)

High blood pressure is the main driver for HHD which increases the arterial pressure of the heart. Left ventricle hypertrophy serves as a kind of compensative or protective mechanism aimed to neutralize the influence of hemodynamic strain on the heart. During systole, the heart muscle contraction in less sufficient, and the functioning heart muscle experiences more wall stress. This localized stress is then transferred into cardiacmyocyte hypertrophy and a decreased volume of the ventricle. With the process continuing, the patient with LVH is likely to suffer more cardiovascular events, including tissue ischemia and the development of arrhythmias.

Fibrosis is another feature of HHD because it is more widespread in the whole heart than in other causes of HF. Fibrosis means that the quality of the cardiac ECM has degraded. The increasing level of type I and type III fibrillar collagen causes an increase in the stiffness of

the myocardium and transforms fibroblasts into stiff myofibroblasts. As a result, it interrupts the contraction and relaxing cycle at both systole and diastole, and the fibrosis causes structural changes in the myocardium, which is associated with dysfunction at systole and further heart failure. The mechanisms of structural changes in HHD remodeling include loss of the normal interaction between the basic components of cardiac ECM, interruptions in the collagen matrix and myocyte slippage.(Berk et al., 2007)

On the other hand, besides hypertrophy remodeling, ventricular dilatation remodeling may happen after AMI. The goal of remodeling is to overcome the loss of contractile tissue and meet the increased metabolic and contractile demands and maintain structural integrity after MI. (Arnal-Pastor et al., 2013) Compared with hypertrophy, the feature of this remodeling is myocyte slippage, thinning of the wall and chamber dilation. In fact, this kind of remodeling also includes fibrosis and myocyte hypertrophy. However, the fibrosis of the initial post-MI remodeling phase just concentrates in the infarcted zone, and the myocyte hypertrophy enlarges the volume of the ventricles instead of increasing the wall thickness. In this case, the ventricular shape changes from elliptical to spherical, and it reduces its ejection fraction and separates the papillary muscles.(Fig 2.2)

The same as for the remodeling of HHD, the motivation for this process is to seek out a protective mechanism. The volume of the ventricle is increased so as to meet the needs of the body. However, this process itself can lead to cell death and pump dysfunction caused by long-term overload. In the adult, cardiomyocytes cannot be reproduced by themselves, and so existing cells have to be expanded (hypertrophy) to realize the increase in volume. (Lindner et al., 2014) With the development of this process, interstitial fibrosis spreads to the

noninfarcted zone, increasing fibrous scar tissue and irreversible spherical ventricular dilation.

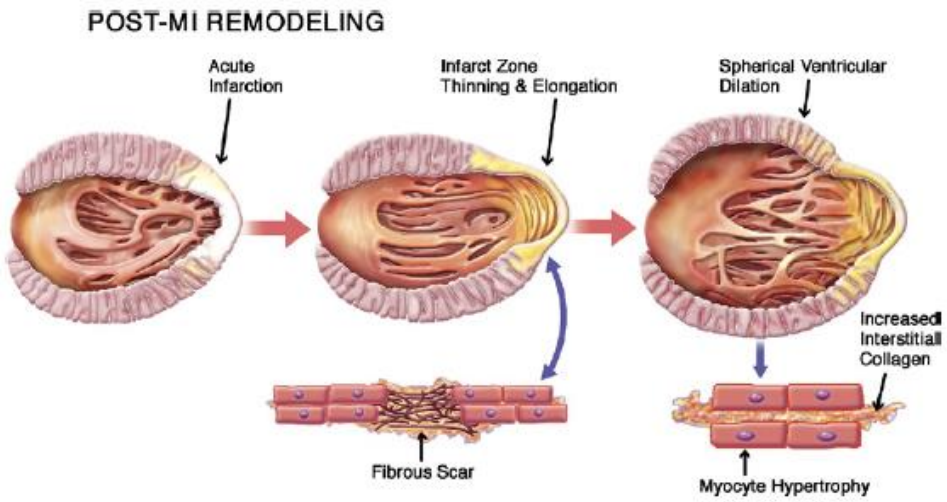

Fig 2.2 Post-MI ventricular remodeling

(Copyright: Marvin A. Konstam , 2010)

These two remodeling mechanisms are always combined and both contribute to significant loss of cardiac function.

What I have discussed above is about the structural changes and physical remodeling of myocardium. However the regulation of the process is always associated with hormones. With a great number of dead myocytes after AMI, the inflammatory response and cytokine elaboration as components of the host response to tissue injury are induced to modulate tissue repair and adaptation.(Nian et al., 2004) Neutrophils, monocytes and macrophages migrate into the ischemic zone to remove necrotic tissue (Sun et al., 2002). The regulation of this

response may be a neurohormonal mechanism that includes the adrenergic nervous system, the rennin angiotensin system and the cytokine system. A variety of proteins such as norepinephrine, angiotensin II, and tumor necrosis factor (TNF) are synthesized to support myofibrous hypertrophy and restore cardiovascular function to a normal homeostatic range. (Mann et al., 1999) Chronically, cytokines such as TNF can mediate repair and remodeling through activating matrix metalloproteinases (MMPs) and collagen formation. In fact, MMPs also have a deleterious effect on the collagen matrix of the heart. Based on that, the consequence of inflammatory cytokine activation leads both to healing, the restoration of function and chronic dilatation that was mentioned above. In this stage, patients remain asymptomatic because the stress-reducing mechanism and the increased blood output is able to meet the demand of the body (Packer et al., 1992). It should be noted that up to 50% LV cardiomytocytes can be lost without inducing heart failure. However, these active molecules do exert a toxic effect on the heart and circulation, and contribute to disease progression.

In fact, after the inflammatory response phase, increasing deposition of cross-linked collagen in the infarcted area replaces the original necrotic tissue with low contractile scar tissue. Studies show that the increased number of autophagosomes which are found in the failing heart suggest an increased autophagic response (Hein et al., 2003). Patients will undergo a transition from asymptomatic to symptomatic heart failure without any prior notice. Once the symptoms are obvious, the damage to the heart is usually irreversible.

Motivated by neurohormonal mechanisms, LV remodeling and cardiomyocyte loss both contribute to insufficient blood supply that doesn’t match the metabolic needs of the cardiac tissues, and so end-stage heart failure occurs. Serious remodeling, insufficient contraction,

low ejection fraction and a large amount of apoptosis provide patients with limited therapeutic options.

2.2 Surgical Therapy

Most surgical therapies in post- AMI can be divided into either artificial device therapy or tissue engineering therapy depending on their specific goals. The aim of artificial device therapy is to assist or replace the function of the heart by an artificial device such as left ventricular assist device (LVAD), a total artificial heart (TAH) or a heart transplant. On the other hand, tissue engineering therapy aims to heal injured heart tissue by implanting specific cardiac, stem or progenitor cells.(Boilson et al., 2010) Certainly, a heart transplant is another therapy for treating heart failure, but the insufficient number of donors, the extremely high expense, the high risk and long-term mortality limit the application of this therapy. (Go et al., 2014) Based on present techniques, there are three different methods for delivering cells to the pathologic region — injection, patch and the use of a restrain device.

2.2.1 Artificial Device Therapy

Left Ventricular Assist Device (LVAD)

LVAD is an electrically driven device that imitates the function of the left ventricle. The ends of the device are connected to the aorta and to the bottom of the LV (Fig 2.3). This device drains the blood from the LV to the aorta and pumps the blood volume in the LV to meet the demands of the body.(Burkhoff et al., 2006)

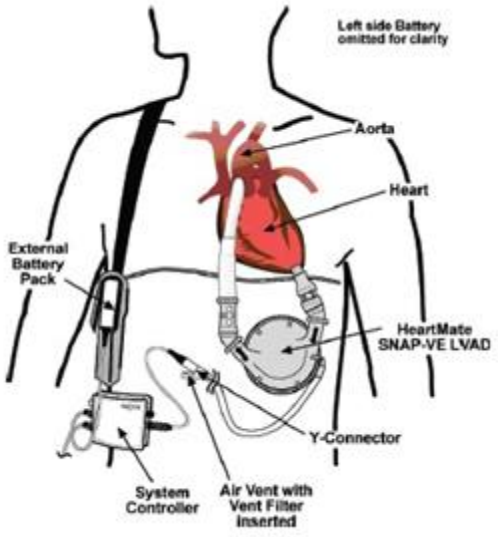

Fig 2.3 Compositions and installation of LVAD

(Copyright: Barry A Boilson,.2010)

Total artificial heart (TAH)

A TAH is another method to treat end-stage heart failure. The mechanism is similar to that of the LVAD, with an electrically driven device imitating the functions of the heart. However, while the LVAD just supports the function of the LV, the TAH totally replaces the heart of the host. The structure of TAH mimics the human heart by consisting of a left chamber, a right chamber and four valves. Both blood pumps and valves control the direction and pace of inflow and outflow (Fig 2.4). This device also needs to connect with other components such as a transcutaneous energy transmission (TET) system, an internal battery and controller so as to support the device's in vivo operation.(Shiva, 2012)

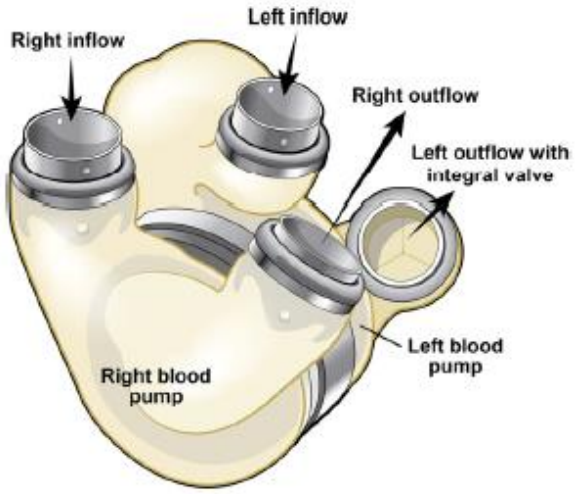

Fig 2.4 Structure of TAH

(Copyright: Shiva M. Sale, 2012)

2.2.2 Tissue Engineering Therapy

Cardiac cell therapy is also known as tissue engineering therapy. The nature of this strategy is to combine different types of cells, biomaterials and signaling molecules so as to regenerate the injured myocardial tissue. These three components play different roles during the healing process. The cells that have the ability to differentiate into specific kinds of cells are the key to the recovery of the injured tissue. The signaling molecules can induce or improve the differentiation process of the cells. The biomaterial is designed to deliver the cells and molecules to the site of interest. During the healing process, it will serve as an artificial extracellular matrix (ECM) and support the cells, protect them, and maintain them. Once the cells have produced enough ECM by themselves, the biomaterial is then expected

to degrade into small, soluble, non-toxic molecules. Another function of the biomaterial is to increase the thickness of the scarred ventricular wall and hence reduce the wall stress. This effect is important to limit the amount of ventricular remodeling and deterioration that is associated with heart failure.(Arnal-Pastor., 2013)

Three common techniques to realize this process as mentioned previously are cell injection, heart patch or scaffold and the application of a heart mesh.(Fig 2.5)

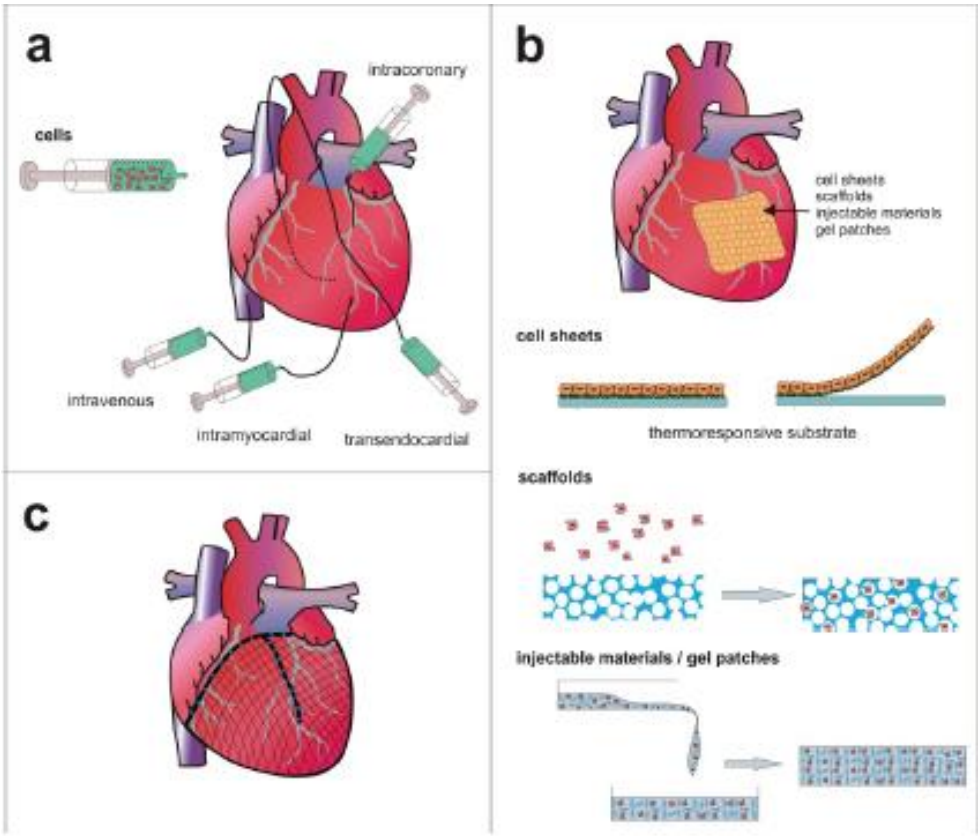

Fig 2.5 Cell therapies

(Copyright: Arnal-Pastor, M, 2013)

Injection

The injection method involves combining the cells with a liquid or gel and injecting them directly into the heart during open-chest surgery. The cells can be injected into different sites such as the intracoronary, intravenous, intramyocardial and transendocardial tissues (Fig 2.5a). A low viscosity solution or hydrogel is used to serve as a carrier for the cells.

Heart mesh

This device is also known as a ventricular restraint device (Fig 2.6). It has been proven to have long-term beneficial impact for patients with heart failure. The Corcap^{TM} cardiac support device is a commercial product made from a polyester warp knitted construction and attached around the ventricles. It can reverse the remodeling process and benefit the CHF for a period of over 5 years.

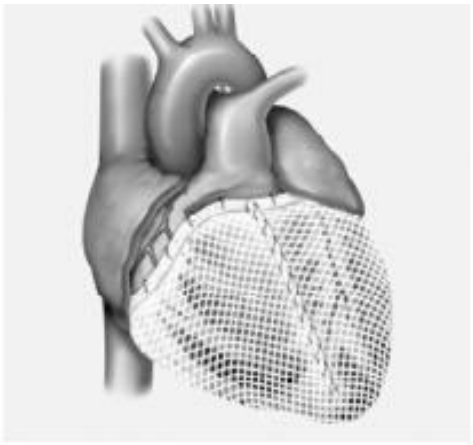

Fig 2.6 Corcap^{TM} cardiac support device

(Copyright: Corcap^{TM})

Heart patch

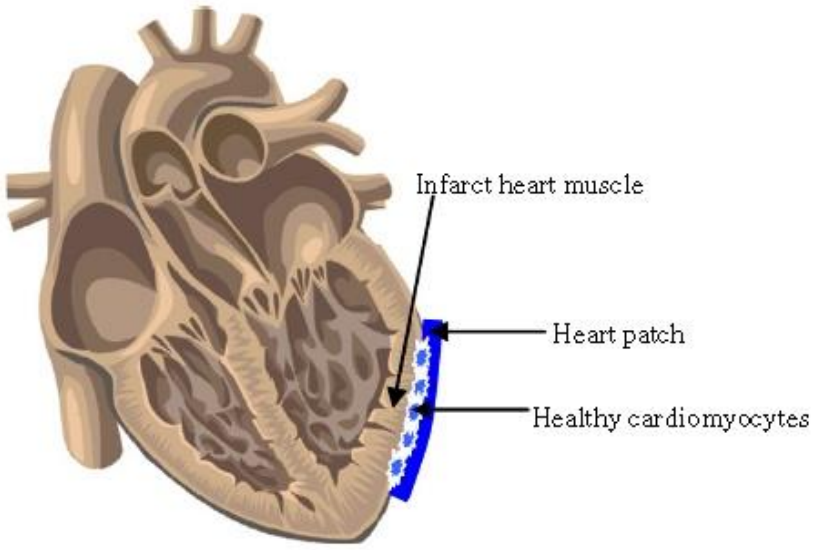

Fig 2.7 Heart patch therapy

(Copyright: Qi-Zhi Chen 2007)

The heart patch or scaffold is a typical tissue engineering strategy (Fig 2.7). Normally, the patch is produced by seeding the specific cell within a three dimensional biodegradable material (Dvir et al., 2011). It can be a kind of thermoresponsive substrate with the cell sheet attached as a separate layer or a three dimensional scaffold with cells seeded inside. This biomaterial scaffold should provide enough structural stability and protection for seeded cells to infiltrate the injured inflammatory environment. Moreover, the material is expected to support the proliferation of the cells and reduce the stress on the heart wall. In summary, the biomaterial needs to have good biocompatibility and similar mechanical performance as the cardiac tissue.

To meet these requirements, some special synthetic materials, biological substrates and gels approved by the Food and Drug Administration (FDA), have been selected to create scaffolds for the culture of cells.

Biological cells and extracellular matrix, including collagen and elastin, can be extracted from the patient by means of a biopsy, and then treated to form a scaffold film or membrane. (Srinivasan et al., 2009) This process takes at least two weeks to complete (Miyagi et al., 2011) due to a series of procedures including extraction, decellularization, expansion and cell seeding. This is too long for patients in an acute state.

For the sake of shortening the preparation time, and in order to maintain the biocompatibility and similar mechanical performance as the relaxed human tissue (Fig 2.8), synthetic biomaterials are currently gaining in popularity as heart patches. Various kinds of cardiac patches are designed to improve tissue regeneration and restrain the remodeling process.

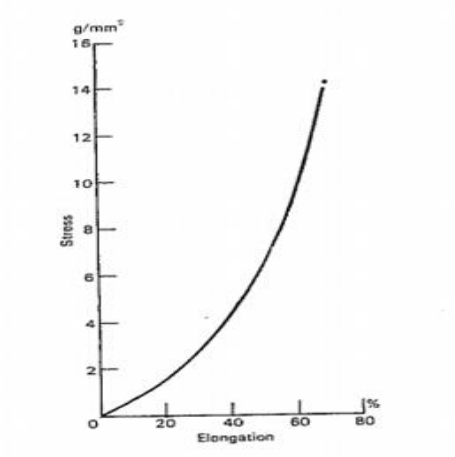

Fig 2.8 Stress-strain curve in tension of human cardiac muscle

(Copyright: Hiroshi Yamada, 1970)

Srinivasan et al proposed that collagen fibers were a promising candidate for use as a cardiac patch. A microbial collagen extraction process was used to extract solid atelopeptide collagen from bovine tendons. Thanks to this process, pure collagen fibers were isolated and the mechanical properties were maintained. A three-dimensional scaffold made from these fibers was suitable for producing a cardiac patch with excellent biocompatibility and mechanical strength.(Srinivasan, A. et al., 2009)

Prabhakaran and her research group developed the "Electrospun biocomposite nanofibrous patch for cardiac tissue engineering". Poly(DL-lactide-co-glycolide)/gelatin (PLGA/Gel) was used to produce the three dimensional scaffold for seeding cardiomyocytes. This kind of scaffold has a lower elastic modulus than a pure PLGA scaffold and integrates cells well in two dimensions. However, compared with the elastic modulus of human myocardium (0.02–0.5 MPa), PLGA/Gel was still too stiff (1.85MPa). (Prabhakaran et al., 2011)

Alternatively, biodegradable polyester urethane urea (PEUU), synthesized polyaniline (sPANi) and poly(glycerol-sebacate) (PGS) have also been selected as advanced materials for cardiac patches. They have been incorporate with proteins, cells and other biomaterials to reduce the stiffness and support the seeded cells.(Fujimoto, K. L.et al 2007) New materials and scaffolds are continually under development, and therefore high compliance and diverse structures make heart patch therapy a popular strategy for treating the injured heart after MI.

2.3 Limitations

2.3.1 Artificial Device and Transplant Strategy

These two LVAD and TAH devices are both designed for end-stage heart failure patients. The literature reports that LVAD can increase the one-year and two-year survival rate by 52% and 23% respectively. After being implanted with a TAH, the life of patients can be extended for several years. Although the benefits of these devices are inspiring, there are some significant limitations we need to take into account. First, the complications and a chronic inflammatory response invariably occur after implantation including a high rate of bleeding, infection, haemolysis and fitting problems. Patients may suffer from the symptoms of anemia and chronic inflammation. (Mankad et al., 2012) Secondly, the devices are very expensive and cumbersome, which can lead to financial problems for the patients' family and influence the daily life of patients. Lastly, some patients who survive a heart attack are not necessarily candidates for LVAD or TAH implantation in spite of deterioration in the injured and remodeling of heart tissue over time. In addition, drug therapy sometimes fails to lower the mortality rate of chronic heart failure (CHF) sufferers. Since the number of donors is limited, heart transplantation fails to meet the actual demand. As a result, cell and biomaterial therapy appear to be a more attractive option.

2.3.2 Tissue Engineering Therapy

Cell therapy is a good alternative for patients who suffer from AMI and who have unacceptable side effects from traditional drug therapy. Favorable results have been reported

based on previous research such as low cost and low immune response. (Segers. et al., 2008) However, there are still some limitations that need to be improved.

The first and the most important issue is the cell survival rate.(Laflamme et al., 2005) The retention of cells after delivery is highly influenced by the delivery route. After intracoronary injection of the cells, typically over 90% of the cells will die within one week. For example, 90% of bone marrow cells can't survive after just two hours. There are various causes for cell loss. It may be due to the low viscosity of the solution that allows them to be washed away immediately by blood flow, or the hostile condition caused by type III collagen and persistent ischemia of the human tissue. The inflammatory environment can also negatively affect the cell survival rate. So these are common challenges of injection therapy.

The second limitation is the time consumption. As mentioned before, it may take several weeks to extract specific cells and collagen from patients or animals. In addition, the generation of a specific tissue construct will take from 11 days to 8 weeks. (Pok et al., 2011) Such a long time influences the economic benefit of heart patches. So the current challenge is to reduce the extraction and culture time for developing new tissue engineered heart patches.(Vunjak-Novakovic et al., 2009)

The last issue is about the mechanical properties. The mechanical behavior of the tissue engineered heart patch is expected to mimic the native tissue. It requires high mechanical stability, good stretch and recovery and similar elastic modulus as cardiac tissue. As I have mentioned above, the present synthetic and biological scaffolds are too stiff compared to cardiac tissue. Although the infarcted tissue of the heart may change from compliant to rigid

after AMI, heart patches are supposed to imitate the healthy native tissue, so they can share the load of the heart during diastole.

For overcoming these limitations, the heart patch should mimic the mechanical properties of native healthy cardiac tissue and the extra cellular matrix so as to support cell attachment and proliferation. The time required to regenerate a tissue construct needs to be minimized so as to increase its potential economic value.

2.4 Knitted Heart Patch

Since a kintted heart patch can deliver cells to the infarcted zone directly and support them in situ, the survival rate of cells is supposed to be higher than that of injection. Furthermore, the mechanical properties of knitted heart patches can be designed and fabricated by changing the knitting methods, stitch notation and other knitting parameters. The time required to prepare a knitted heart patch is relative short, and the production efficiency and yield are much higher than for traditional non textile tissue engineering scaffolds.

2.4.1 Scaffold

In previous research studies, several kinds of knitted fabric have been applied as cardiac patches. Dacron (polyester) fabric has frequently been used for patching cardiac defects for myocardium restoration and the repair of atrial septal defects in sheep. (Radisic et al, 2008) However, this kind of knitted patch has been criticized by many researchers for its poor mechanical performance, significant inflammatory response and insufficient biocompatibility. As a result, knitted patches fabricated from alternative biomaterials are

highlighted with their desirable biological, biomechanical and chemical properties. (Kochupura et al., 2005)

Ozawa et al developed a kind of biodegradable scaffold for use as a cardiac graft made from ε-caprolactone-co-L-lactide sponge reinforced with a knitted poly-L-lactide (PLLA) fabric. The knitted fibrous portion provided sufficient mechanical support, and it took one to two years before complete resorption. According to Ozawa's research, it provided "an optimal biomaterial for the creation of autologous cardiac grafts". (Ozawa et al., 2002)

Jan Bouclik et al also developed a kind of biodegradable elastomeric knitted fabric for treating heart remodeling. Hyaluronan benzyl ester was extruded into microfilaments to make multifilament yarns, and then the yarns were processed into fabric using a circular weft-knitting machine. After that, the fabric was folded in two to form the two layer scaffold. The weft knitted structure (Fig 2.9) ensured the elasticity of the scaffold, and the mechanical properties were suitable for in vivo implantation. Their findings about the influence of attached cells and fibrin on the mechanical properties warranted further research on assessing the functionality of this scaffold as a heart patch. (Boublik, et al, 2005)

Fig 2.9 Structure of knitted heart patch

(Copyright: Jan Boublik, 2005)

2.4.2 Materials

There are several strict requirements for the materials used to form the heart patch since they are attached to the myocardium directly. The material should meet the following requirements.

1. It should be biodegradable and biocompatible.
2. The yarns of the material should have adquate mechanical properties to be knitted, and they should be strong enough to prevent continuation of the remodeling process.
3. The material should promote the proliferation and migration of the cells along the fiber.

Poly-L-lactic acid has been employed extensively as an ecological material for cartilage repair, surgical suture fabrication, as an implant material, and as a scaffold for tissue

regeneration. It has been approved by the FDA for use as a suture material and for orthopedic repair as bone plates and screws. The properties and process of PLA have been investigated and reported over the last decade (Garlotta, 2001). The tensile properties, crystallinity, microstructure, and melt preparation have been researched, and the optimal parameters for the industrial production and development of new applications of PLA have been reported. Moreover, various methods can be applied to change the properties of PLA including surface modification for use in specific applications such as tissue engineering. (Lopes et al., 2012) The mechanical properties of PLA fabrics can also be modified by using different textile fabrication technologies such as electrospinning, knitting, weaving and braiding.

As mentioned before, poly-L-lactic acid is one form of PLA which has been found to be suitable as a biomaterial for a knitted cardiac patch. It has been able to provide sufficient mechanical support and biodegrades slowly over time.

Moreover, PLA can copolymerize with other monomers to improve the biological and mechanical performance. For an instance, poly(lactic-co-glycolic acid) (PLGA) has also been used to fabricate a biomimetic cardiac patch incorporating either an ePTFE Teflon^{TM} component (Chen et al., 2014) or carbon nanofibers (CNF).(Asiri et al., 2014) In fact, PLGA, as the copolymer of poly(lactic acid) (PLA) and poly(glycolic acid) (PGA) has been used in various FDA approved devices for bone, nerve and skin repair.

In summary, PLA should be a promising biomaterial for this study based on the results and conclusions from previous research. It also appears to meet all the requirements for a cardiac patch.

2.4.3 Cells

Another critical component of tissue engineering a heart patch is the source of cells. The cells used to repair the infarct site on the heart are expected to meet several requirements. One obvious requirement is the function of the cells including differentiation potential and controllability of proliferation. Due to the inability of an intrinsic repair mechanism to restore the function of the ventricles after MI, the delivered cells should have the capability to drive the reestablishment of myocardial structure and vascular perfusion, which means that the cells should provide a source of various cells types, such as myocytes, cardiac fibroblasts and vascular endothelial cells. At the same time, uncontrollable differentiation and over-proliferation must be avoided. The delivered cells should induce angiogenesis as well as the necessary myogenesis while avoiding proliferation after generating sufficient number and density of cells. To reduce the risk of the hyperplasia, the types of cells are selected based on the results from in vitro and in vivo tests.

The culture environment for the cells at the site of an infarction is an issue that needs to be considered when selecting cells. As mentioned before, the adverse condition caused by persistent ischemia and the inflammatory environment will negatively influence the attachment and proliferation of cells at the infarct site.

Multiple cell resources including bone marrow mononuclear cells (BM-MNC), embryonic stem cells (ESC), mesenchymal stem cells (MSC), induced pluripotent stem cells (iPS) and cardiosphere-derived cells (CDCs), are increasingly popular in applications of tissue engineered devices. All these stem cells can be expanded in vitro and have proven to have a positive influence on myocardial restoration.(Vunjak-Novakovic, G.et al,2009)

In this study, CDCs were selected as the delivered cells. This is because it has been confirmed that the clonogenicity and multilineage potential of CDCs can provide "the greatest functional benefit for repairing experimentally induced myocardial infarctions" (Li et al, 2012)

Cardiosphere-derived cells are a mixture of cardiac stem cells and supporting cells, derived from an endomyocardial biopsy.(Smith et al., 2007) In order to obtain a sufficient number of CDCs, expansion of the endomycardial biopsy involves mincing the explants into 1 mm sized fragments and plating them in suspension culture. (Fig 2.10) The explants in suspension culture are self-assembled into three dimensional cardiospheres. Then the cardiospheres are replated in culture flasks to yield the prespecified dose of CDCs. At the present, the clinical delivery method for the CDCs involves injecting the cells directly into the infarcted site.(Makkar et al., 2012)

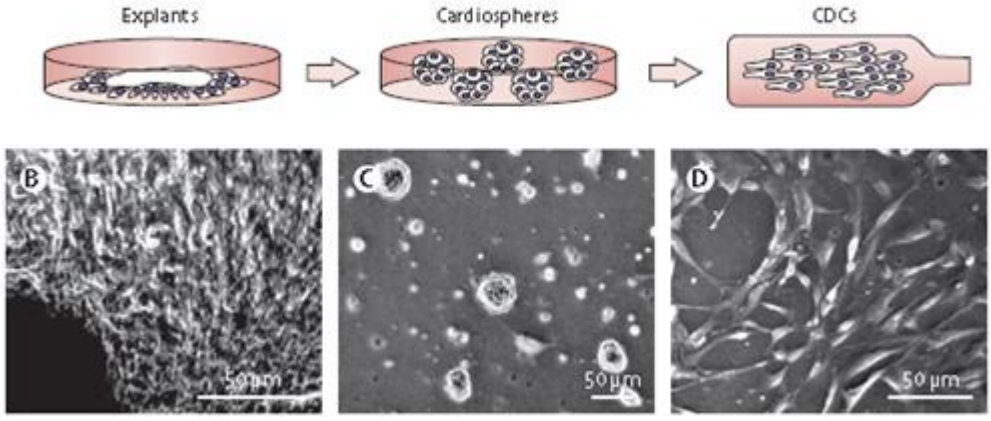

Fig 2.10 Cultural process of CDCs

(Copyright: Raj R Makkar, March 2012)

Based on the results of in vivo tests, the heart function of the patients who received CDCs is significantly improved compared with the control group. Specifically, the research showed that the CDCs significantly improved the function and reduce the extent of injury of the left ventricular myocardium, including a reduction in the infarct size and scar mass (Fig 2.11a,b), improved mechanical properties of the myocardium (Fig 2.11c) and increased thickness of the wall of the left ventricle. This means that adverse remodeling of the infarction site was limited or prevented. (Johnston., et al, 2009)

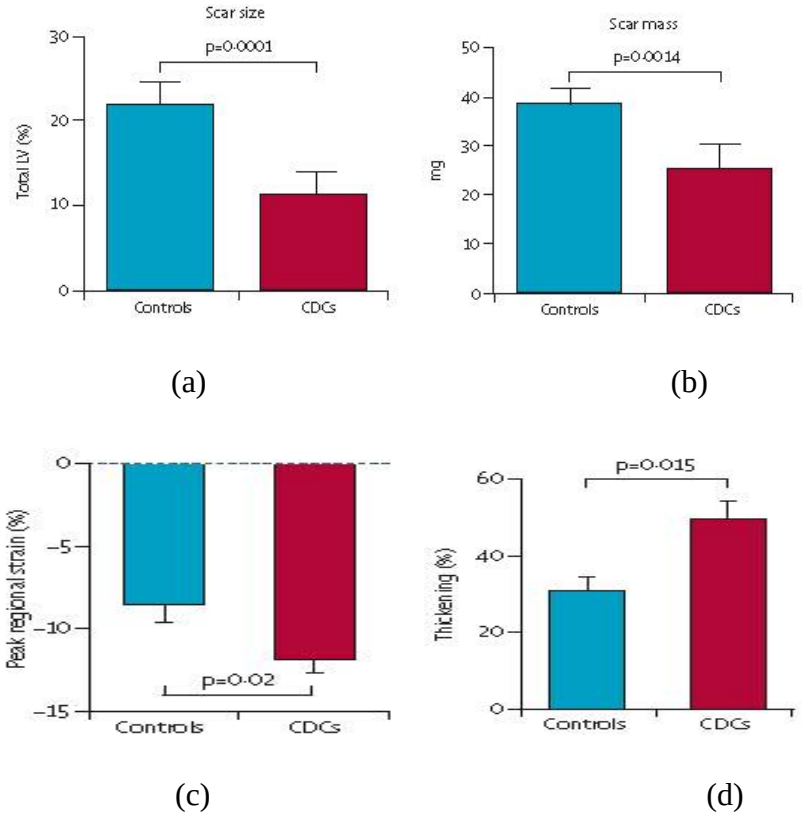

Fig 2.11 Myocardial regeneration in rats treated with and without CDCs
(a) Scar size, (b) Scar mass (c) Peak strain (d) Change in thickness of myocardium
(Copyright: Raj R Makkar, March 2012)

Compared with MSC's and BM-MNC's, the CDCs exhibited a unique ability to generate a balanced paracrine factor production. Increasing evidence supports the fact that the regeneration process of myocardium depends mainly on the guidance of paracrine mechanisms. Various paracrine productions are able to enhance the regeneration of specific kind of cells, such as fibroblasts and hepatocytes. In another words, the amount and type of growth factors that the stem cells can secrete determines the regenerative ability of the stem cells. According to the recent research, "CDCs are unique in their ability to secrete large amounts of a wide range of growth factors compared with other stem cells" (Li et al., 2012) This includes angiopoietin-2, basic fibroblast growth factor (bFGF), hepatocyte growth factor (HGF), insulin like growth factor (IGF-1), stromal cell-derived factor (SDF-1) and vascular endothelial growth factor (VEGF).(Fig 2.12)

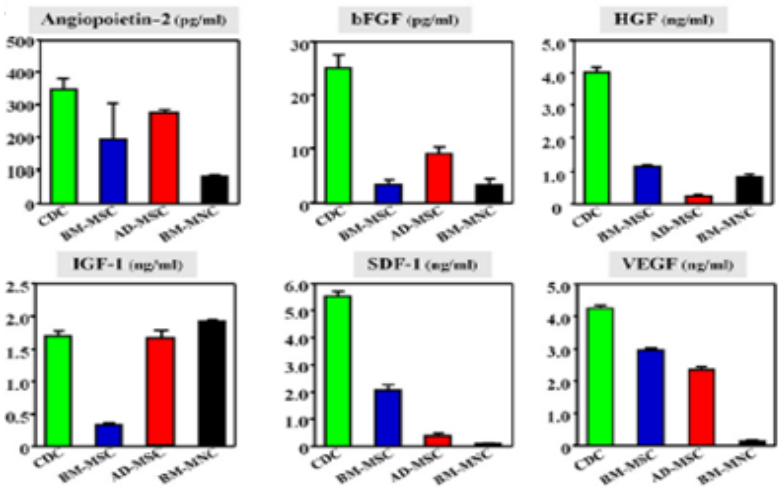

Fig 2.12 Concentration of growth factors secreted by different types of stem cells

(Copyright: Tao-Sheng Li,2012)

To sum up, the CDCs are a promising choice for myocardium regeneration.

2.4.4 Structure

Based on the previous research on PLA (Garlotta, 2001), its tensile strength can reach 60 MPa, and its tensile modulus can exceed 3 GPa, which is much higher than that of myocardium which boasts only 3-15 kPa and 0.02-0.5MPa respectively. (Chen et al 2007) Since PLA is such a stiff material, it is the structure of the cardiac patch which plays a critical role in defining the patch's mechanical behavior. To mimic the mechanical properties of the human tissue, some researches have formed a thin film (McDevitt, et al 2002) or a three dimensional electrospun nanofiber web (Prabhakaran et al,2011) so as to achieve adequate porosity and a sufficiently low modulus.

The process of yarn knitting is a traditional technique recently introduced to tissue engineering applications and biomedical devices. The features of a knitted fabric are its high porosity, outstanding flexibility and superior durability. Biomedical textiles have successfully focused on hernia meshes, vascular grafts and sutures, for which they have proven able to meet the dynamic in vivo mechanical requirements and support the regeneration process. Moreover, due to their superior biostability, these devices continue to function as permanent implants for many years, equivalent to the life expectancy of the patient.

With respect to the knitting fabrication technique, knits can be divided into weft knitted structures and warp knitted structures depending on the shape, type and sequence of loops incorporated into the design.

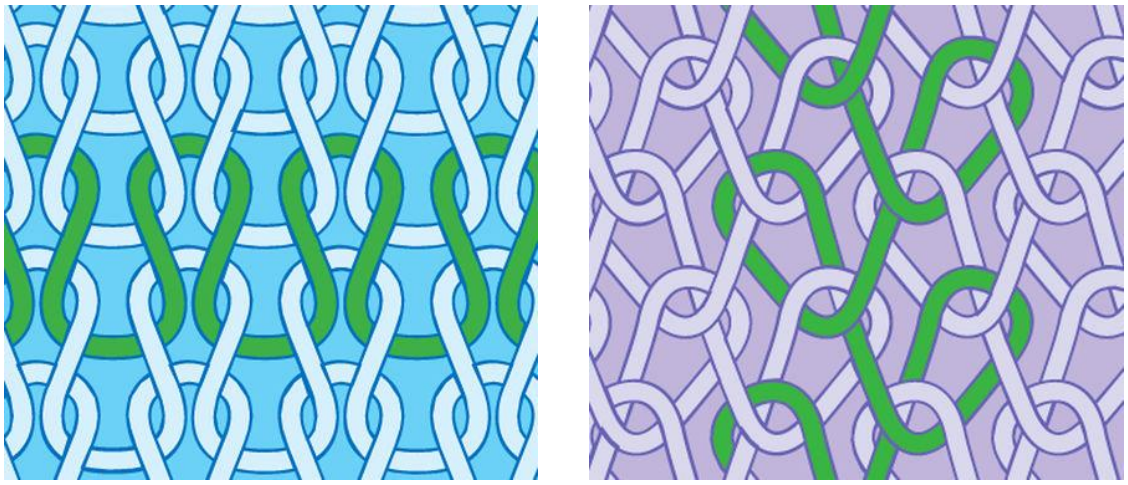

(a) (b)

Fig 2.13 Loop structure of (a) weft knitted and (b) warp knitted fabrics

(Copyright: Sarah Veblen, 2008)

After analyzing the mechanical properties of weft knitted and warp knitted fabrics, the relative amount of strain for weft knitted fabrics is inevitably higher than that of warp knitted fabrics in both directions, while they both enjoy high levels of porosity.

Type	Source	Dimension	Extension	Porosity	Merits and demerits
Woven	Yarns	Stable	Low	Low	To unravel easily at the edges when cut or trimmed
Knitted					
Weft	Yarns	Unstable	High	High	Additional yarns are utilised to interlock the loops
Warp	Yarns	Stable	Versatile	High	Having flexibility and inherent ability to resist unravelling
Braided	Yarns	Stable	Middle	High	The yarns criss-cross each other
Nonwoven	Fibres	Varying	high	Varying	Determined by those of the constituent polymer or fibre and by the bonding process

Fig 2.14 Features of textile structures

(Copyright: Wang X , 2011)

The loop structure of weft knitted fabrics is more flexible, which means lower stiffness, great compliance and less dimensional stability. Given these features, weft knitted fabrics could simulate the mechanical properties of native tissue and support cell migration and proliferation. In addition, they have been employed as reinforcing structures for skin mesh and small diameter vascular prostheses due to their outstanding compliance.(Ng and Hutmacher, 2006) However, there are some disadvantages of weft knitted fabrics such as raveling, curling and creep phenomena. To overcome the propensity to curl and their dimensional instability, weft knitted fabrics are heat set so as to ensure that the fabric is flat, smooth and uniform.

In this study, the primary goal of designing the cardiac patch is to mimic the performance of the cardiac muscle and support the migration and proliferation of CDCs at the infarct site. A weft knitted structure appears to be the best choice for fabricating the heart patches. Moreover, due to the high modulus of PLA yarn, the weft knitted structure is believed to be an appropriate method to create a compliant and low modulus fabric from inherently stiff yarns.

CHAPTER 3

MATERIALS AND METHODS

3.1 Fabrication of Cardiac Patch

3.1.1 Materials

The structure of poly-L-lactic acid is shown in Figure 3.1. The Type 6400D PLA polymer was purchased from NatureWorks LLC (Minnetonka, MN). Due to the presence of an ester group, PLA or PLLA is initially a hydrophobic polymer. However, when exposed to water or biological activation *in vivo*, it is readily degraded into lactic acid.

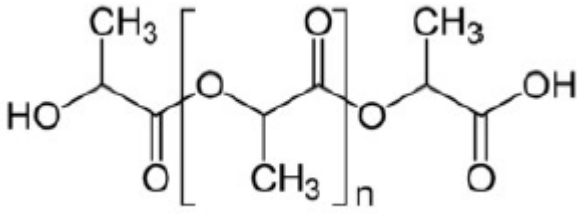

Fig 3.1 Chemical structure of PLA

The reason why PLA was selected as the raw material for fabricating cardiac patches is because of its abundant clinical experience. Poly-L-lactic acid has been used in orthopedic applications such as sutures, and it has been approved by the Food and Drug Administration

for a number of different applications. Its biodegradability and biocompatibility as an implantable device has been approved on numerous occasions.

The PLA yarns used in this study were obtained from Fiber Innovation Technology Inc (Johnson City, TN), where they were melt spun and drawn during a customized run to prepare a 150 denier as-spun yarn and a 81 denier drawn multifilament yarn with 48 filaments, round filament cross-section and 1.7 denier per filament. The basic information and properties are listed in Table 3.1. The cross section of the filaments is round as can be observed in Figure 3.2.

All the fabric samples in this study were knitted using a 4-ply PLA multifilament 324 denier, yarn on a Shima Seiki Model SWG021N flat V-bed knitting machine in the College of Textile, NCSU.

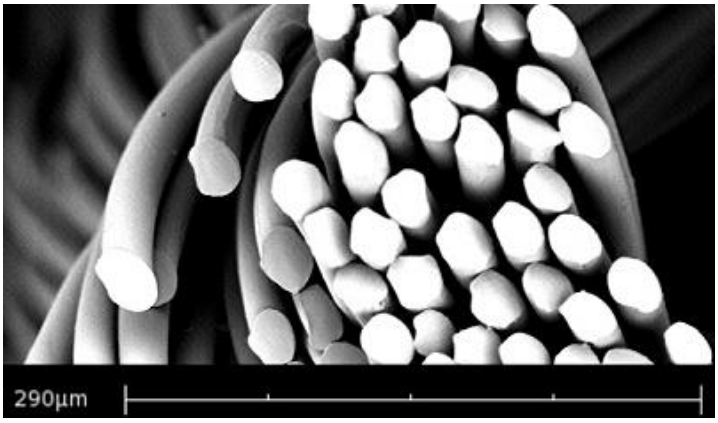

Fig 3.2 Cross section of PLA filaments

Table 3.1 Properties of PLA fiber and yarn

Properties of PLA Fiber and Yarn	
Density (g • cm^{-3})	1.21-1.43
Glass transition point (Tg) (℃)	40-70
Melting point (Tm) (℃)	130-180
Ultimate tensile strength (MPa)	53
Tensile modulus(GPa)	3.4
Number of yarn plies	4
Number of filaments per yarn	192
Denier of yarn	324
Cross section of filament	Round

(Ratner B, 2013)

To avoid any degradation of PLA caused by exposure to the humid ambient environment, the knitting process was completed within one week. After knitting, the fabrics were scoured with 2% non-ionic surfactant (Triton X-100) at room temperature for 20 minutes and then rinsed with deionized water in order to remove any dirt, oil and contaminants on the fabric's surface.(Wu, 2012) Since weft-knitted fabrics have a tendency to curl along their edges, which may affect the measurement of the stability of their structure, heat setting was applied to flatten the fabrics and stabilize the structure. As a result, the fabrics were thermally set in a Werner Mathis hot air oven with edges fixed on a pin frame at 55℃ for 5 min to eliminate

curling and minimize changes in the mechanical properties after scouring and pre-drying in a spin dryer in the College of Textiles Pilot Laboratory. After heat setting, all the fabric samples were sealed in paper envelopes to limit degradation and were stored in a clean vacuum desiccator until further tests and treatments.

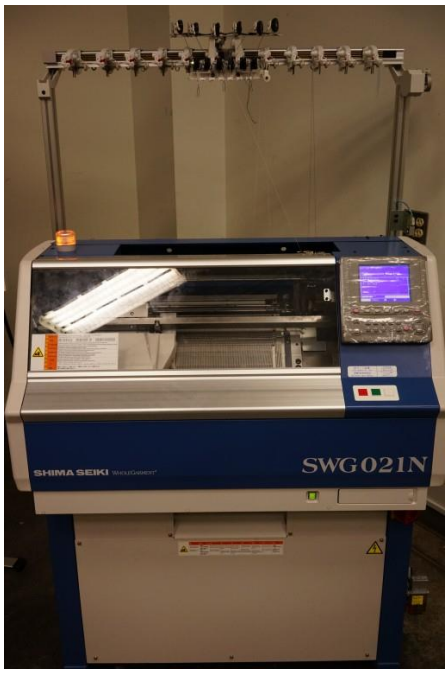

Fig 3.3 Shima Seiki SWG021N weft knitting machine

Fig 3.4 Werner Mathis hot air oven

Polyethylene terephthalate (PET) fabrics

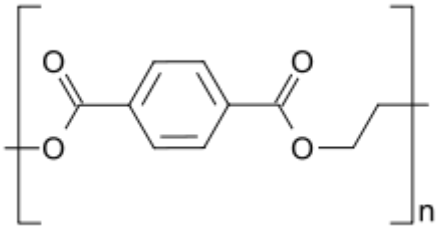

Fig 3.5 Chemical structure of PET

Polyethylene terephthalate is extensively used to fabricate biomedical devices. With an initial tensile modulus of 3.0-4.9 GPa and an ultimate tensile strength of 42-80 MPa, the tensile properties of PET are similar to those of PLA. Moreover, by using a PET yarn linear density of 70 denier, this was close to that of the PLA yarn with a linear density of about 80 denier. Based on these characteristics, PET was selected as the initial material of choice to fabricate

the preliminary prototypes and determine which weft knitted structures could closely imitate the tensile properties of myocardium. A Shima Seiki weft knitting machine (Model SWGO21N) was used to fabricate the samples. Once the prototype structures were fabricated and the "candidate" samples had been selected, the same knitting parameters were applied to weft knit the PLA fabrics.

3.1.2 Weft Knit Structures

Several representative textile structures were weft knitted from polyester yarns prior to selecting certain types of stitches for knitting the PLA cardiac patch samples. For most prototype samples they were knitted with folded 2-ply PET yarn.

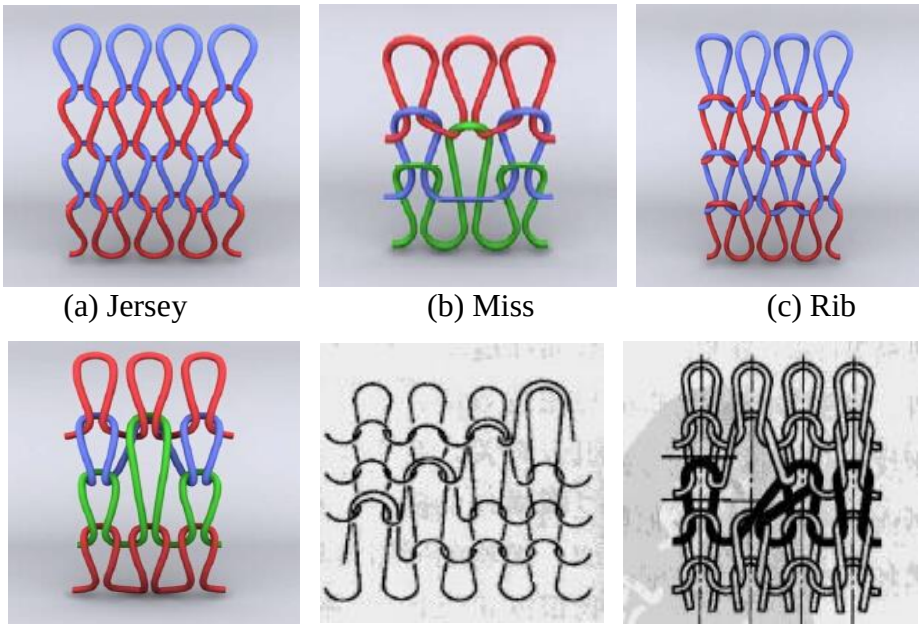

(a) Jersey (b) Miss (c) Rib

(d) Tuck (e) Twill (f) pointelle

Fig 3.6 Stitch notation of weft knitted prototype fabrics
(Copy right: AATCC, North Carolina State University 2008/ Hairu Long, 2008)

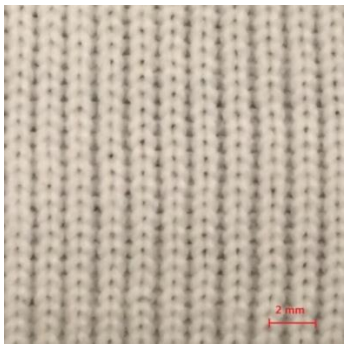

(a) Jersey

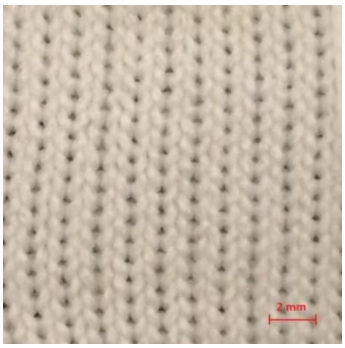

(b) Miss

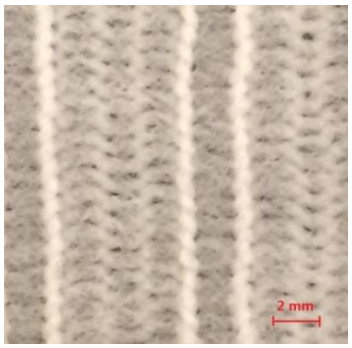

(c) Rib

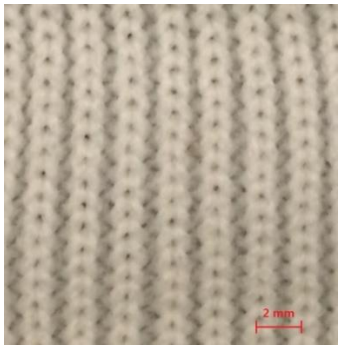

(d) Tuck 1

(e) Tuck 2

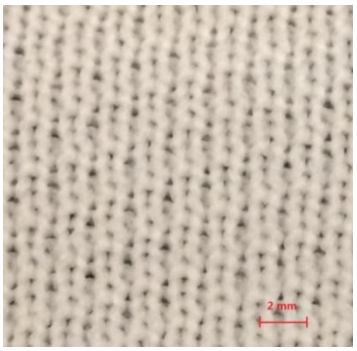

(f) Twill

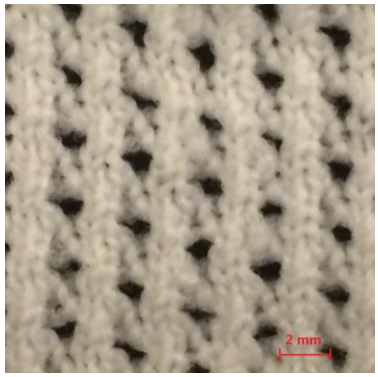

(g) Pointelle

Fig 3.7 Structures of weft knitted prototype fabrics

The stitch notations and structures of the fabrics are shown as Fig 3.6 and Fig 3.7.

For four of the specific stitch types one end of spandex yarn was added to the 2-ply polyester feed yarn making it folded 3-ply yarn supply. As a result, the jersey, tuck, miss and pointelle samples were knitted with both a 100% polyester and a polyester/spandex yarn in order to improve the elasticity and decrease the initial modulus of these particular stitch structures. The mechanical performance of these blended fiber samples was compared with those of the 100% polyester samples with the same stitch structures so as to determine the effect of the spandex yarn component.

3.2 Morphology and Mechanical Evaluation

3.2.1 Thickness Measurements

Both thickness measurements and values for the mass per unit area were required in order to calculate the total porosity of the knitted prototype fabrics. The porosity is known to be a major factor to influence the migration and proliferation of cells through the knitted scaffold. The thickness was measured with a thickness gauge (SDL 94, Shirley Developments Ltd, Stockport, England) according to ASTM D1777-96 Standard Test Method for Thickness of Textile Materials. (Fig 3.7)

The fabric was compressed by a series of applied weights (175g, 350g, 525g, 700g) and the thickness value was recorded at each of these pressures. The relaxed thickness of the sample was then determined by extrapolating the linear thickness to pressure relationship to zero applied weight.

Fig 3.8 SDL thickness gauge

3.2.2 Porosity Calculation

Porosity is a critical characteristic for many different biomedical textile products. It is defined as "the percentage of void space within the boundaries of a material compared to its total volume, which is the sum of the solid matter and the void space."(Guidoin, 1986)

The total porosity of any textile fabric can be calculated from the equation:

$$P = 100\left[1 - \frac{M}{1000hd_f}\right],$$

where M= mass per unit area of the fabric (g m^{-2})

h = fabric thickness (mm)

d_f = fiber density (g cm^{-3})

This equation has subsequently been adopted by ASTM F2450-10 (Standard Guide for Assessing the Microstructure of Polymeric Scaffolds for Use in Tissue-Engineered Medical Products). The density of the PLA polymer in this study is assumed to be 1.24 g/cm^3 (Liang, 2013), whereas the density of the PET polymer is assumed to be 1.38g/cm^3. In order to measure the mass per unit area, each fabric was cut into 1cm × 1cm slices and weighed on an electronic balance to the nearest 0.1 mg.

3.2.3 Uniaxial Stretch and Recovery Test

The uniaxial stretch and recovery cyclic tensile test described in ASTM D 5035-11, Standard Test Method for the Breaking Force and Elongation of Textile Fabrics, was followed using a crosshead speed of 10 mm/min (the same speed for the recovery process) and an initial gauge length of 1 inch (25 mm). Specimens from all the knitted samples were cut to a length of 2 inch (50 mm) to be long enough to be clamped in the top and bottom jaws.(Lu, 2014) The width of the specimens was 1 inch (25 mm), which was equivalent to the length of each specimen. The jaw width was maintained at 5 mm. It is known that variations in the test method will influence the accuracy and precision of the experimental results. “The effect of variability on the test parameters should be reduced as much as possible”.(Dabiryan, 2013) Prior to tensile testing, the fabrics were heat set and flattened so as to remove any wrinkles and residual tension in the knitted samples.

Five repeated cycles were set as the pre-test condition to remove any relaxation that occurred

to the knitted and heat-set fabrics. The crosshead speed for the stretch and recovery test was set at 10 mm/min and the maximum percent strain was set as 20%. This is where the Young's modulus was measured, and then the jaws would be returned to the original position at the same speed. The load at 20% strain and change of the load during both the tensile stretch and recovery steps were recorded. Based on the dimensions of the specimen and the results of the test, the Young's modulus was calculated using the following equation:

$$E=\text{tensile stress/tensile strain}=\sigma/\varepsilon=\frac{F/A}{\varepsilon}$$,(Lu, 2014)

Where E is Young's modulus (MPa), F is the tensile force applied on the specimen (N), A is the cross-sectional area of the specimen, and the ε is tensile strain, which in this test is 20%.

The tester was a uniaxial Instron® Mechanical Tester, Model 2712-864 and the load cell capacity was 5N (Figure 3.9). Bluehill 2.0 Material Testing Software was used to record and analyze the results. Five specimens were tested for each sample.

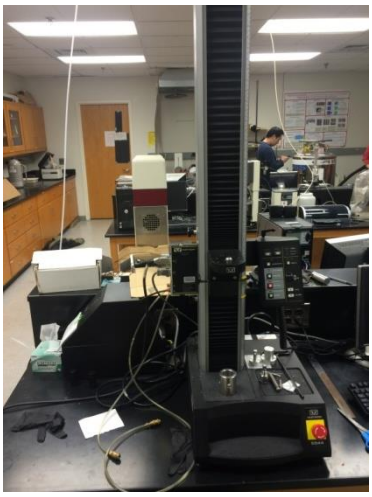

Fig 3.9 Tensile test on the uniaxial Instron® testing machine

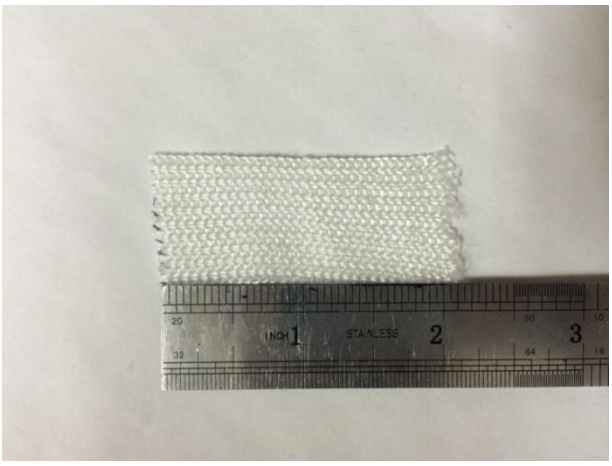

Fig 3.10 Specimen preparation for uniaxial stretch and recovery test

The tensile and recovery test was done in both the warp (vertical) and weft (horizontal) directions. These directions are shown as the Fig 3.11.

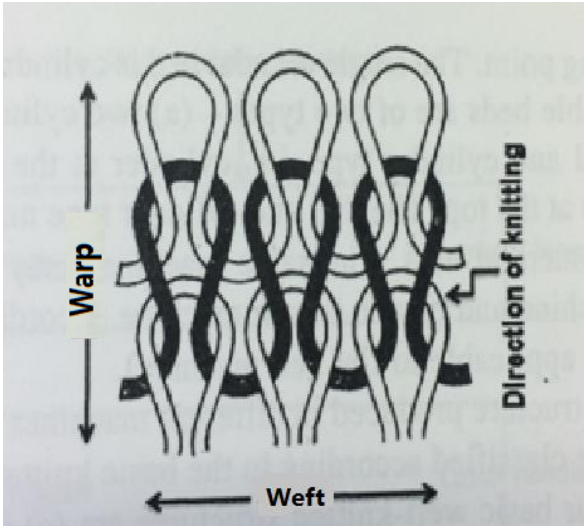

Fig 3.11 Warp (vertical) and weft (horizontal) directions of weft knitted fabric

(Copyright: Ray, S. C. 2012)

3.2.4 Biaxial Stretch and Recovery Test

The biaxial stretch and recovery test measured the state of stress simultaneously in both directions. All the knitted samples were cut into 10mm × 10mm square specimens. The test area was 6mm × 6mm, the other 4 mm regions were used to mount the specimens in the jaws. The true strain was set at 20% and the rate of displacement was set at 10 mm/min, which was the same speed as for the uniaxial Instron machine. Five pretest cycles were applied to minimize any relaxation phenomenon. When the warp (vertical) direction was stretched, the weft (horizontal) direction was fixed by the jaws during the test, and the forces in both directions were recorded for further analysis at 10 Hz, and vice versa, which means that when the weft direction was tested, the warp direction was fixed. After stretching and elongation, the jaws were returned at the same rate.

The biaxial tester was a CellScale Biomaterial Testing BioTester 5000 Master Controller with 0.5 N load cell. The camera of the tester recorded the images during the tests at 5 Hz. LabJoy(Version 9.15) image analysis software was used to review and analyze these images. (Fig 3.12)

(a) CellScale BioTester

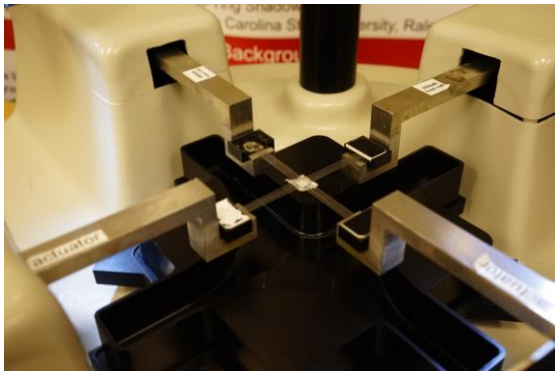

(b) Jaws of the biaxial tester

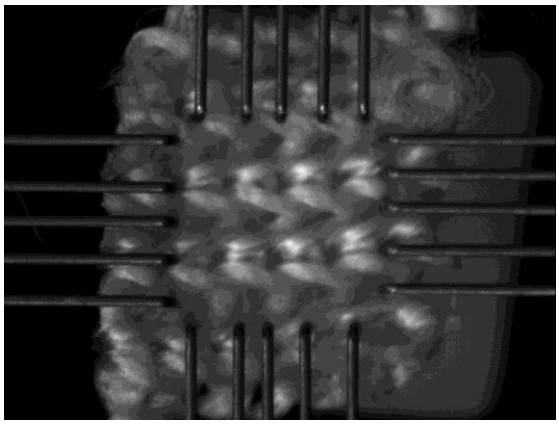

(c) Biaxial specimen set up

Fig 3.12 Biaxial stretch and recovery test

3.3 Biology Performance

3.3.1 Sample Preparation

Six mm diameter discs were punched out of all the samples and placed in a 24-well plate. Each disc was put in a single well. A total of ten specimens were prepared for each kind of

sample. Out of the ten, four specimens were used for Day 0 of the MTT assay, four for Day 7 of the MTT assay and two for SEM testing.

Samples were sterilized in 70% ethanol overnight and placed in a hood followed by three serum-free DMEM washings.(Di Bella et al., 2008) Prior to use, the discs were dried in a clean desiccator.

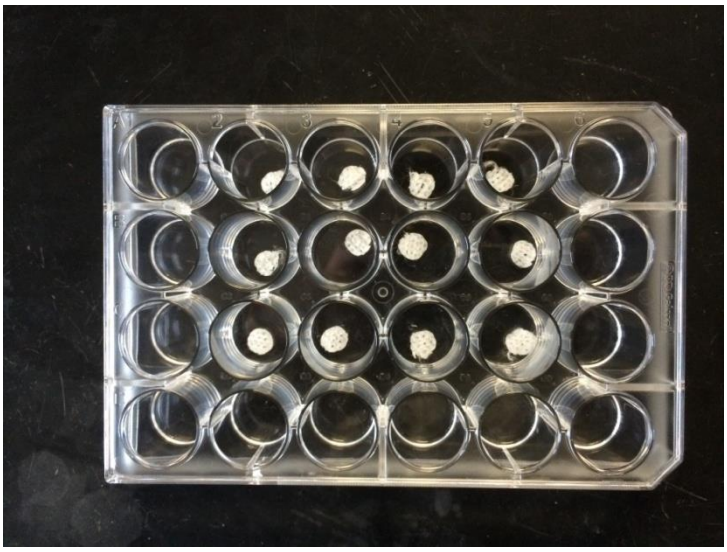

Fig 3.13 PLA knitted scaffold specimens measuring 6 mm in diameter

3.3.2 Preparation and Harvesting of Cardiosphere-derived Cells (CDCs)

The CDCs cell line was extracted from the ventricles of 2-year old beagle dogs in the College of Veterinary Medicine, North Carolina State University. The passage number was one, and the date the cells were frozen was 14th December 2014. The concentration of cells was 3×

10^6/ml. The complete culture media was composed of 78% IMDM (Iscove's Modified Dulbecco's Media, high glucose) with phenol red, 20% FBS (Fetal Bovine Serum, Atalanta®), 1% L-glutamine (Invitrogen®25030-164), 0.5% Gentamycin (Gibco,15710-064) and 0.5% 2-Mercaptoethanol (Invitrogen 21985-023). The cells were stored under nitrogen until the experiment began. All procedures were completed in a biosafety cabinet so as to maintain strict aseptic conditions throughout the biological experiment. First, the bottom of a T-75 flask needed to be coated with fibronectin to facilitate the attachment of the CDCs. 125µl of frozen fibronectin (BD Bioscience, 356008, 1mg/ml) was thawed and diluted in 4.875ml distilled water (Invitrogen 10977) to make 5 ml of a coating solution. The 5 ml coating solution was added to the T-75 flask that was gently rocked back and forth to ensure that every part of the bottom was covered. This was followed by placing the flask in a 37℃ incubator for at least 30 minutes before using. Secondly, the CDCs were added to the T-75 flask for cell expansion. Media was pre-warmed in a 37℃ water bath, and the water was aspirated from the fibronectin treated T-75 flask followed by washing with 10 ml PBS (phosphate-buffered saline). Then the fibronectin treated T-75 flask with 15 ml culture media was incubated at 37℃ in 5% CO_2 for at least 15 minutes, and the T-75 flask with media was retrieved from the incubator and the CDCs were transferred into it. The media was changed every 48 hours. Third, cell passage was required when confluence had reached approximately 80%. The cell passage included harvesting cells, counting cells and subculturing cells.
At the beginning, media was aspirated from the T-75 flask followed by 5 ml PBS washing followed by the addition of 5 ml Tryple Select (Gibco,12563-029) to detach the cells from

the bottom. The flask was incubated at 37℃ for 5 min. Then an optical microscope was used to confirm the detachment of the cells. (Detachment could be improved by gently rock the flask.) Once the cells were detached, 5 ml culture media was added, and then all the solution was collected in a sterilized centrifuge tube. Another 5 ml media was added to wash the flask and collected in the same tube. The yield and viability of the cells was checked by means of a hemacytometer with Trypan blue. The cell solution was redistributed into 7.5×10^5 cells in total. Then, it was centrifuged at 410 relative centrifugal force (rcf) for 5 minutes. After taking the centrifuge tube out, the supernatant was removed from the centrifuge tube, and the pellet of cells was left. The pellet of cells was then resuspended in 1 ml media.

Finally, the cell solution was added to the fibronectin coated T-75 flask with 14 ml culture media.

The T-75 flask was returned to the incubator at 37℃ and 5% CO_2.

3.3.3 Coating of Cardiac Patch Scaffold

The coating solution was composed of 250µl fibronectin (1mg/ ml) diluted in 4.75 ml serum-free DMEM. (Dulbecco's Modified Eagle Medium, Gibco 12491-015). A 600µl coating solution was added to each well prior to immersion of the PLA discs. Fibronectin was absorbed at the surface of PLA discs during incubation at 37℃ overnight followed by washing in serum-free DMEM. Prior to seeding the cells, all discs were washed by PBS.

In 24 well culture plate, two wells were selected as the control group and coated with fibronectin. A 600 µl coating solution was added into each well and incubated overnight.

3.3.4 Seeding CDCs on Cardiac Patch Scaffold

The target cell seeding concentration was 1×10^5 cells per disc. Two 24 well culture plates with PLA discs were sterilized and coated with fibronectin prior to use following the above protocols. One plate was used to conduct an MTT assay at Day 0, and the other was used for the Day 7 MTT assay and SEM photography.

1. When confluence had reached 80%, the CDCs cells were harvested from the T-75 flask, and they were transferred to a conical tube.
2. The total number of cells was counted using a hemacytometer, and the total required number of cells was calculated. Thirty four wells were needed; thirty for the PLA discs and four control wells. Each well was seeded with 1×10^5 cells, so the total number of cells required was 3.4×10^6. The required volume of solution was transferred into a centrifuge tube, and centrifuged at 410 rcf for 5 minutes.
3. The supernatant liquid was removed from the centrifuge tube, so just the pellet was left. The pellet was then resuspended in 3.4 ml media to ensure the density of cells reached 1×10^6 cells/ml.
4. 100 µl cell solution (1×10^5 cells) was added on the center of each disc in order to improve the cell attachment to the scaffold instead of on the bottom of the well. For the control group well, 500 µl culture media combined with 100µl cell solution was added to each well. After that, the culture plates were incubated for 30 min to allow the cells to attach to the scaffold.
5. After half an hour, 500 µl culture media was added to each well.

6. The Day 0 plate was left in the hood to conduct the MTT assay. The Day 7 plate was returned to the incubator.

3.3.5 Cell Proliferation by MTT Assay

Reduction of 3-(4,5-Dimethylthiazol-2-yl) -2,5-diphenyltetrazolium bromide (MTT) provides a simple, accurate and reliable method to measure the extent of cell proliferation. MTT can be reduced by active mitochondria in living cells, and also the pale yellow tetrazolin MTT will be converted into purple formazan crystal which can be solubilized and spectrophotometrically quantified.

First, a vial of MTT powder (10mg Sciencell 8028a) was reconstituted with 2 ml PBS, shaken briefly and filtered through a 0.2 μm filter to prepare an MTT stock solution. Second, the media in a 24-well culture plate with phenol red was vacuum aspirated, and the scaffolds were washed with DMEM without phenol red. Third, all the discs were transferred to a new 24 well culture plate. 500 μl of DMEM with no phenol red and 50μl MTT stock solution were added into each well including the control group, mixed by rocking the plate gently side to side. Then the 24 well culture plate was incubated at 37 ℃ for 4 hours. Fourth, given that black crystals formed with living cells, 300 μl media was removed from each well followed by adding 250 μl of MTT solubilization buffer solution. (Sciencell 8028b). The solution was pipetted up and down to help dissolve the crystals. Then, the dish was incubated at 37 ℃ for ten minutes and gently mixed to enhance dissolution.

After the MTT formazan dissolved, 100μl of solution was transferred from each well to a new 96 well plate. (Twelve wells in the 96 well plate were used for each kind of specimen, 6

wells for the control group, 6 wells for the negative control, and 6 wells were blank.) Finally, the absorbance of the medium was measured at a frequency of 540 nm in a Synergy (Biotek model:SIAFER) micro-plate reader.

Fig 3.14 Synergy micro-plate reader

3.3.6 Cell Attachment by Scanning Electron Microscopy

The extent of cell attachment to the PLA scaffolds was evaluated after 7 days of culture by scanning electron microscopy (SEM). The discs of knitted PLA scaffold with CDC cells were prepared for SEM as follows. First, most of the culture media was removed, and the cells were fixed at 4℃ in 3.0% glutaraldehyde plus 1% sucrose in 0.1 M sodium phosphate at pH 7.0 overnight. Second, the discs were washed three times in 0.1 M sodium phosphate, and stored at pH 7.0 at 4 ℃. Third, all the discs were dehydrated through a graded series of

aqueous ethanol solutions which included 30%, 50% and 70% for 15 minutes at 4 ℃ at each concentration. After dehydrating in 70% ethanol, the discs were immersed in 95% ethanol for 30 minutes followed by dehydrating in 100% ethanol three times, thirty minutes each. The last two changes were done at room temperature for critical point drying. Third, critical point drying was conducted by a critical point dryer (Samdri®-795) for 10 minutes at the critical point (Fig 3.15a). After mounting the discs on stubs which have been prepared with carbon dots, the discs were placed in a desiccator overnight. Fourth, the discs were sputter coated with gold/palladium in a Hummer® Model 6.2 sputter coater to generate a 25 Å thick coating on their surfaces (Fig 3.15b). The prepared PLA scaffold discs were then viewed in a JEOL Model 5900 LV scanning electron microscope with a 15 kV accelerating voltage to observe the extent of cell attachment.

(a) Critical point dryer

(b) Sputter coater

(c) JEOL scanning electron microscope

Fig 3.15 Equipment for SEM viewing

3.4 Statistical Analysis

The means and standard deviations of all the results were calculated using a SPSS-22 software program. As the ANOVA test can calculate the variance of the means for each group, it was utilized to do statistical comparisons between the group means. If the p-value was ≤ 0.05, the difference between the mean values between groups would be considered significant and a standard t-test would be introduced to analyze the difference between two individual groups. If the p-value was ≤ 0.05, the difference between the two groups would therefore be assumed to be statistically significant.

CHAPTER 4

RESULTS AND DISCUSSION

4.1 Knitting Structure Selection Based on PET Samples

All the initial prototype PET samples, except for the jersey 1E stitch sample, were successfully knitted using two ends of polyester 70 denier multifilament yarns. In order to select the "candidate" structures for knitting the heart patches out of PLA yarns, the total porosity, Young's modulus and stress-strain curves of each PET sample were measured and compared between groups and against human myocardial tissue to determine which structures were suitable for further research.

4.1.1 Total Porosity

The following equation from Chapter 3 was applied:

$$P = 100\left[1 - \frac{M}{1000hd_f}\right]$$

where M is mass per unit area of the sample in $g.m^{-2}$, h is the thickness in mm and d_f is the fiber density in $g.cm^{-3}$.

The total porosity of all the polyester (PET) samples ranged from 84.15% (Jersey 2E) to 92.26% (Rib). In this equation, the thickness and mass per unit area are variable factors that influence the total porosity, while the fiber density remains constant at 1.38 $g.cm^{-3}$. The thickness of the samples ranged from 0.77mm to 1.69mm due to the different number of feed yarns. The jersey 1E stitch structure was knitted from just one end of PET yarn, and the

spandex blended samples were fabricated from two ends of PET yarn together with one end of spandex yarn. The rest of the samples were knitted by folding two ends of PET yarn together and using them as one feed supply without twist.

To get the mass per unit area, the samples were cut into 5cm ×5cm squares and weighed on an electronic balance to a precision of 0.1 mg.

Table 4.1 Structural properties of the PET knitted samples

	Thickness(mm)	Mass per unit (g/m^2)	Porosity (%)
Jersey 1E	0.77	101.84	90.35
Jersey 2E	0.91	199.02	84.15
Tuck 1	1.24	213.90	87.50
Tuck 2	1.25	212.35	87.70
Pointelle	1.21	191.73	87.60
Rib	1.21	129.17	92.26
Twill	1.04	194.96	86.42
Miss	1.22	227.16	86.45
Pointelle_spandex	1.33	191.27	89.15
Miss_spandex	1.69	248.00	88.97
Tuck1_spandex	1.59	224.44	89.39
Jersey_spandex	1.34	197.71	88.86

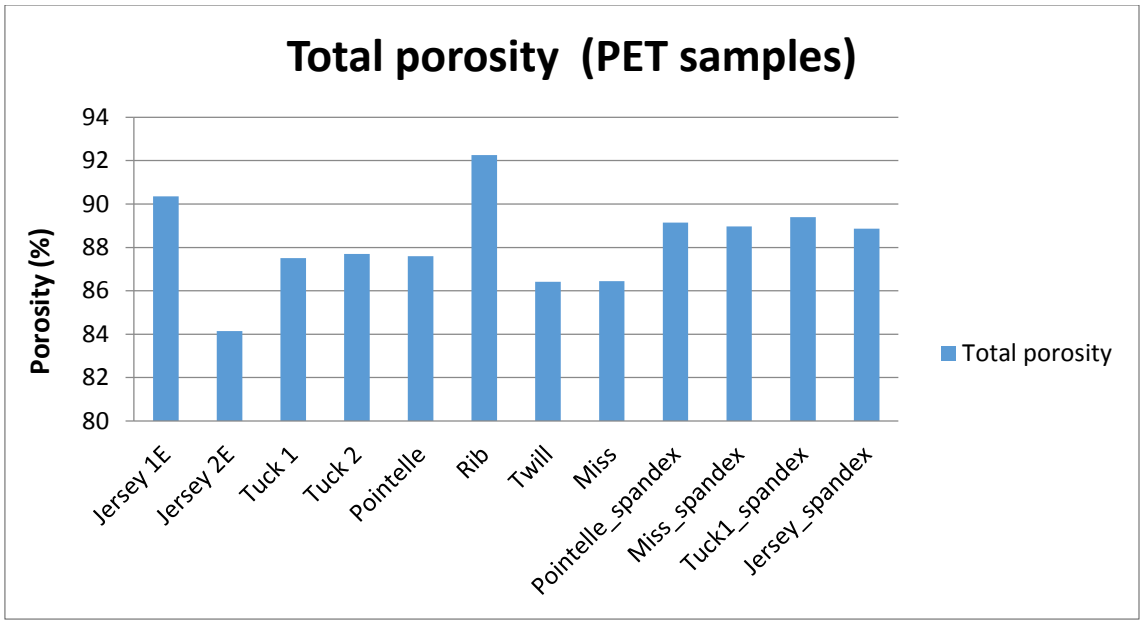

Fig 4.1 Total porosity of the PET knitted samples

The total porosity is a critical factor which influences the nutrient supply and oxygen exchange inside the fabric. Higher porosity means that it can provide more channels to exchange nutrients, oxygen and cell metabolites, and in addition the cells can migrate from the surface to the interior more easily through the thickness of the fabric scaffold. Fabrics with high porosity can theoretically improve the proliferation and survival rate of cells. As a result, the rib stitch appears to be the most promising choice for seeding cells, and the jersey 2E stitch may be the least attractive.

4.1.2 Mechanical Properties

The Young's modulus and tensile stress-strain curves are the most direct methods for measuring the mechanical properties of the samples. In this study, the Young's modulus and

the uniaxial tensile stress-strain curve for the warp (vertical) and weft (horizontal) directions of each sample were compared with that of myocardial human tissue to determine the differences and similarities between them.

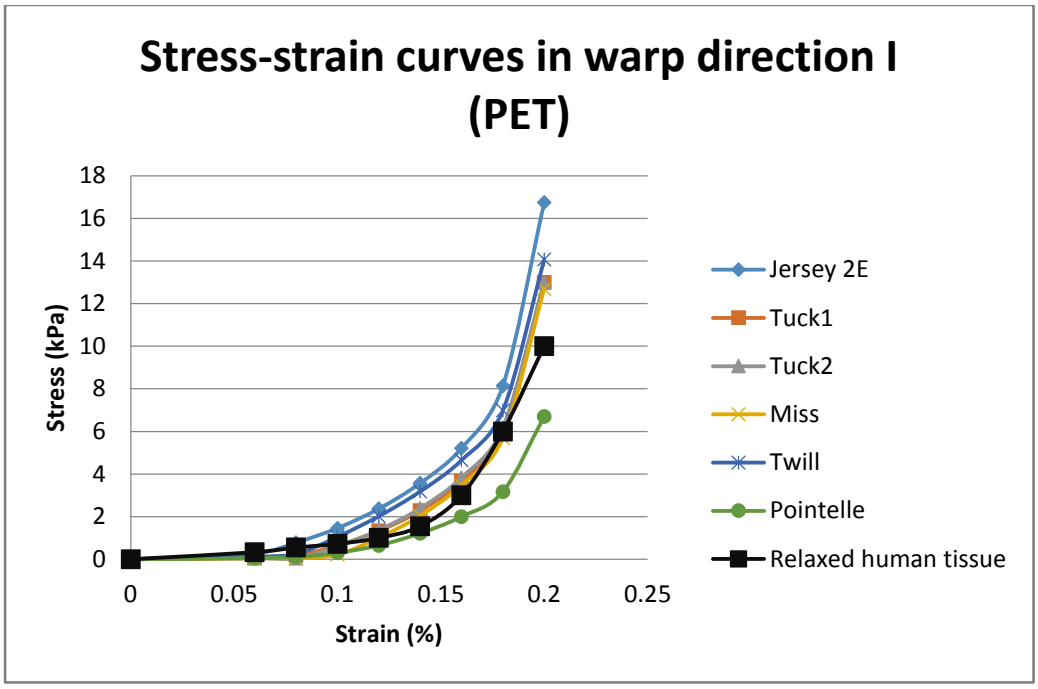

(a)

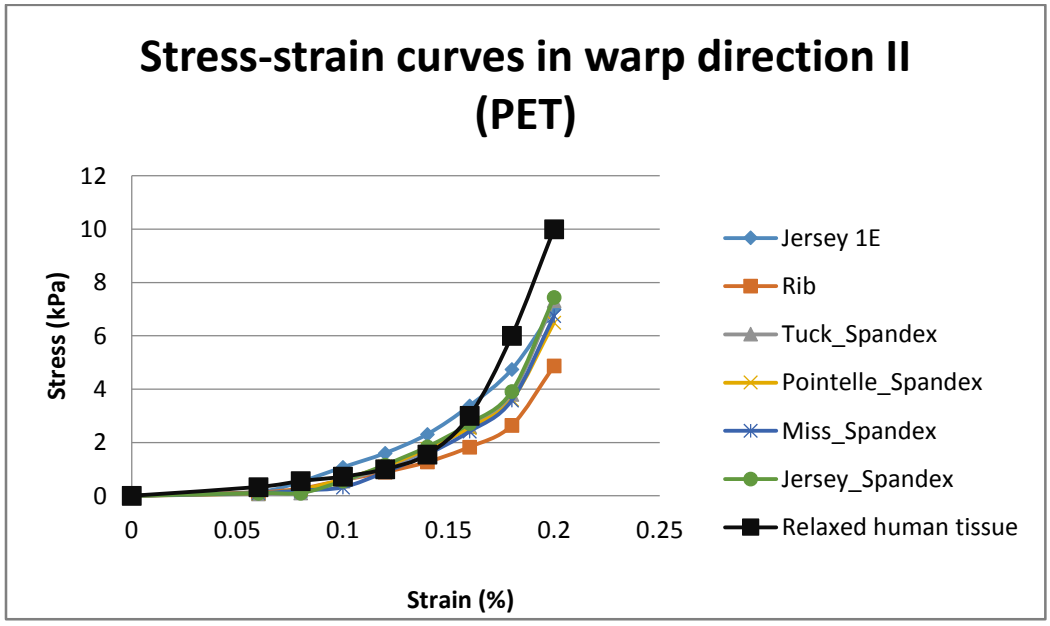

(b)

Fig 4.2 Stress-strain curves of PET samples in warp (vertical) direction

Based on the previous literature (Chen, 2008)(Yamada et al., 1970), the stress of relaxed human myocardium was about 10 kPa at the beginning of diastole. Meanwhile, the stiffness of the myocardium can reach 200 kPa at the end of diastole. The non-linear elasticity of this relaxed human tissue stress-strain curve is shown in Fig 4.2. This particular shape of stress-strain curve is difficult to reproduce using solid homogenous synthetic and natural materials and has posed a challenge for the biomaterials scientists in the past. However, it is evident from Fig 4.2, that most of the knitted samples can mimic the curve of myocardial host tissue in the warp direction.

All the PET scaffold samples were divided into two groups; those that were stiffer than relaxed human tissue and those that were more compliant. Based on Fig 4.2a the curves for the jersey 2E, tuck1&2, miss and twill stitches are above the natural tissue curve, which means that they have higher stiffness and a higher stress under the same strain than relaxed human tissue. On the other hand, the curves for the jersey 1E, rib and pointelle stitches are below that of the relaxed human tissue curve (Fig 4.2a and Fig 4.2b), which means that they are less stiff and more compliant.

By adding the spandex yarn, the stiffness of all the samples appeared to decrease except for the pointelle stitch sample. Although the difference is not significant in all cases based on an ANOVA statistic ($p > 0.05$), the stress for the jersey, tuck and miss stiches at 20% strain decreased by over 50 % after adding the spandex yarn. For the pointelle stitch structure, the mechanical performance remained at the same level.

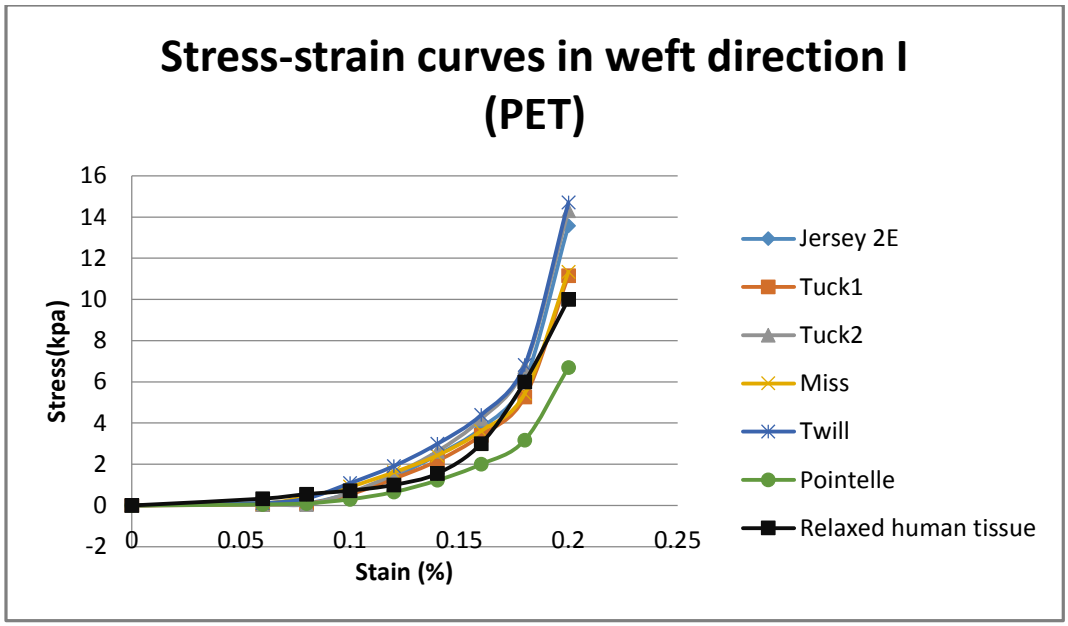

(a)

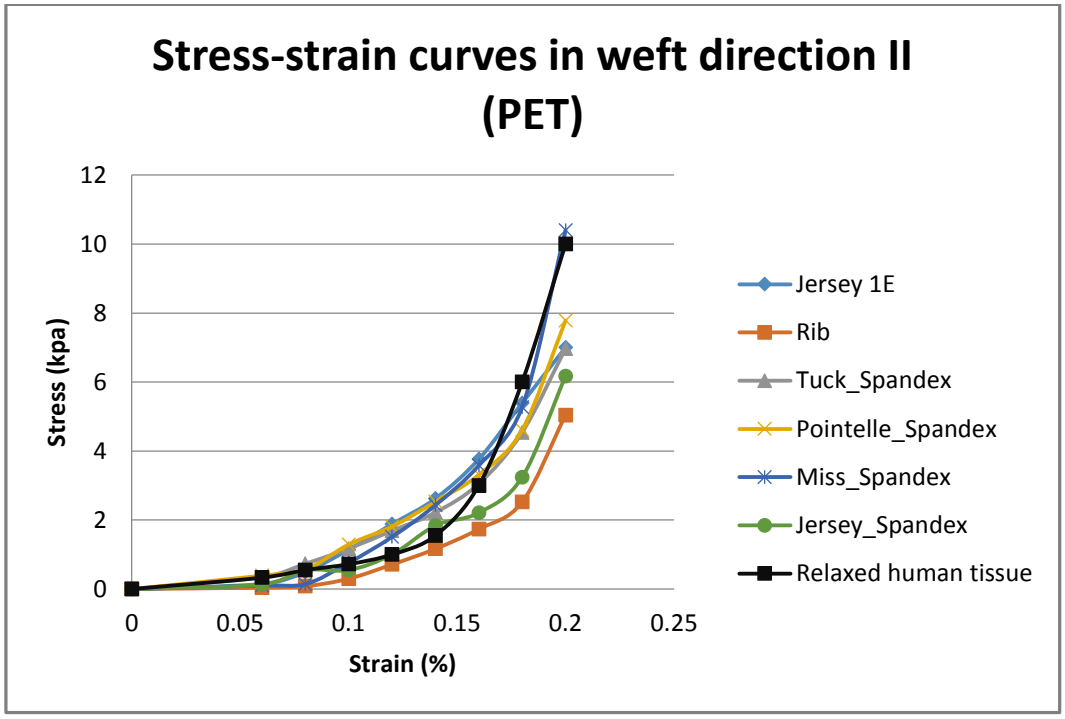

(b)

Fig 4.3 Tensile stress-strain curves of PET samples in weft (horizontal) direction

A similar result occurred for the tensile tests in the weft direction. Again the mechanical properties of the relaxed human tissue were mimicked by the weft knitted polyester structures. There is a tendency for weft knitted structures to curl up once the fabric is no longer under tension due to the different residual yarn tensions on the face and back of the fabric, and the extent of curling depends on the particular type of stitch, the size and type of knitted yarn and the stitch frequency. During tensile testing, the curl and curved loop shape of the stitch in the warp or weft direction become distorted as the yarns become aligned and more parallel. In this segment, the amount of strain is contributed mainly by the knitted structure. As the strain increases, the yarns move closer to each other and the width of the specimen shrinks. Once the yarns are stretched and become straight, the mechanical properties of the structure depend almost entirely on the mechanical characteristics of the yarns themselves.

This is the reason why during the uniaxial tensile tests the stiffness of knitted fabrics was low at the beginning of the test, and why it increased rapidly after a certain amount of strain. Moreover, the amount of curl, the stitch frequency and the tightness of the yarns in the warp and weft directions were different. That is why both directions were tested so as to determine the potential for mechanical support of the myocardium in both directions.

Because the spandex yarn had a much lower modulus than the polyester (PET) yarn this resulted in lower stresses being experienced by the spandex samples during the latter stages of the test. However, the spandex yarns were still combined with the PET yarns in the same knitted loops. The amount of decrease is marginal, as shown in Fig 4.2 and Fig 4.3.

Table 4.2 Young's modulus of PET samples

	Young's Modulus (kPa)	
	Warp (vertical) direction	Weft (horizontal) direction
Jersey 1E	35.00	35.00
Jersey 2E	83.75	67.90
Tuck 1	64.95	55.75
Tuck 2	65.00	71.50
Pointelle	33.50	33.50
Rib	24.35	25.20
Twill	70.35	73.55
Miss	63.50	56.70
Pointelle_spandex	32.50	33.50
Miss_spandex	33.75	52.00
Tuck1_spandex	36.60	34.85
Jersey_spandex	37.20	30.85
Relaxed human tissue	50.00	50.00

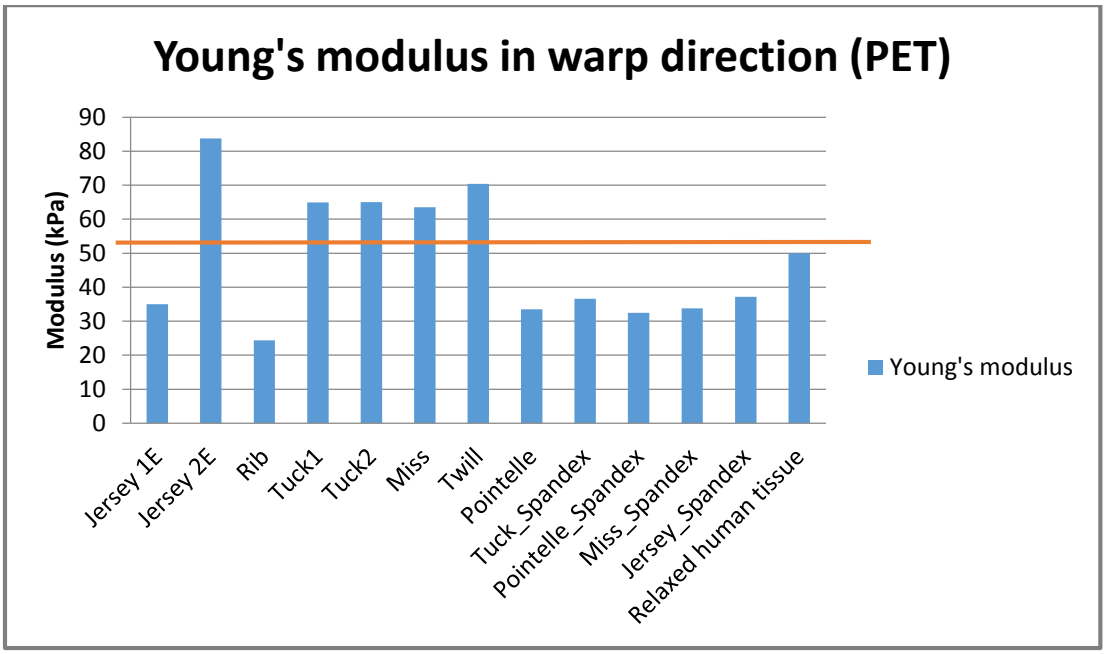

(a) Warp (vertical) direction

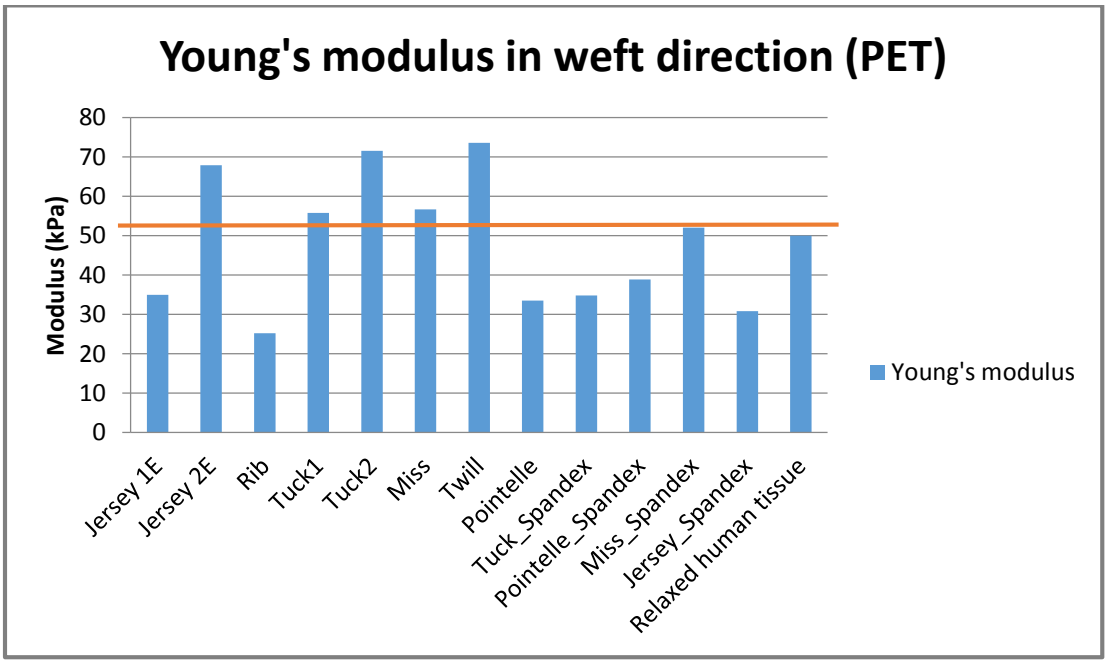

(b) Weft (horizontal) direction

Fig 4.4 Young's modulus of PET samples

Based on the literature (Chen Q et al,2008) (Yamada H,1970), the Young's modulus of human myocardial tissue is about 50 kPa at 18% strain. According to Fig 4.2 and Fig 4.3, the stiffness of most samples increases rapidly during the last 2% elongation. In this study, 18% strain was set as the point to compare the Young's modulus between the prototype weft knitted samples and human myocardium.

The Young's modulus of the PET samples ranged from 24.35 kPa to 83.75 kPa in the warp direction and 25.2 kPa to 73.55 kPa in the weft direction as presented in Table 4.2. Fig 4.4a) shows that the jersey 2E, tuck 1&2, miss and twill stitch structures had higher moduli than the relaxed human tissue in the warp direction. And the situation was the same in the weft direction except for the Young's modulus of the miss_spandex sample, which exceeded that of the natural tissue in the weft direction.

Through analyzing the stress-strain curve and modulus of each PET samples, the jersey 2E, tuck1 and rib stitch structures were selected as the preferred "candidates" for fabricating heart patches from PLA yarns. The spandex samples were abandoned for several reasons. Firstly, spandex polyurethane is not a polymer that is approved by the FDA for any implantable end-use. It is known to degrade *in vivo,* but the degradation by-products have been found to be cytotoxic. So it is likely to lead to toxic adverse events if implanted on or near the heart. Secondly, the original motivation for adding spandex to the polyester weft knitted structures was to improve the compliance and elasticity, and decrease the stiffness of certain weft knitted structures so as to mimic the mechanical properties of the myocardial host tissue. However, the results from the stretch and recovery test showed that most structures knitted from PET yarns were able to generate a similar stress-strain curve and Young's modulus to

that of the relaxed human tissue. Finally, the ANOVA statistical analysis confirmed that the difference between the polyester and spandex samples was not significant. In summary, none of the spandex samples were selected.

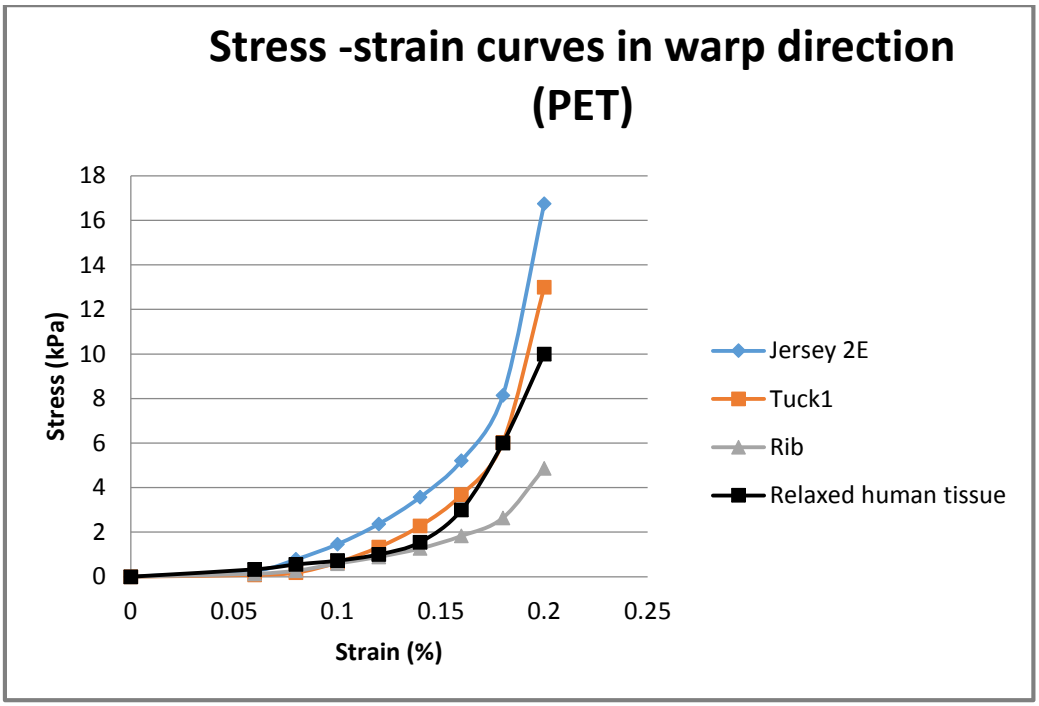

(a) Warp (vertical) direction

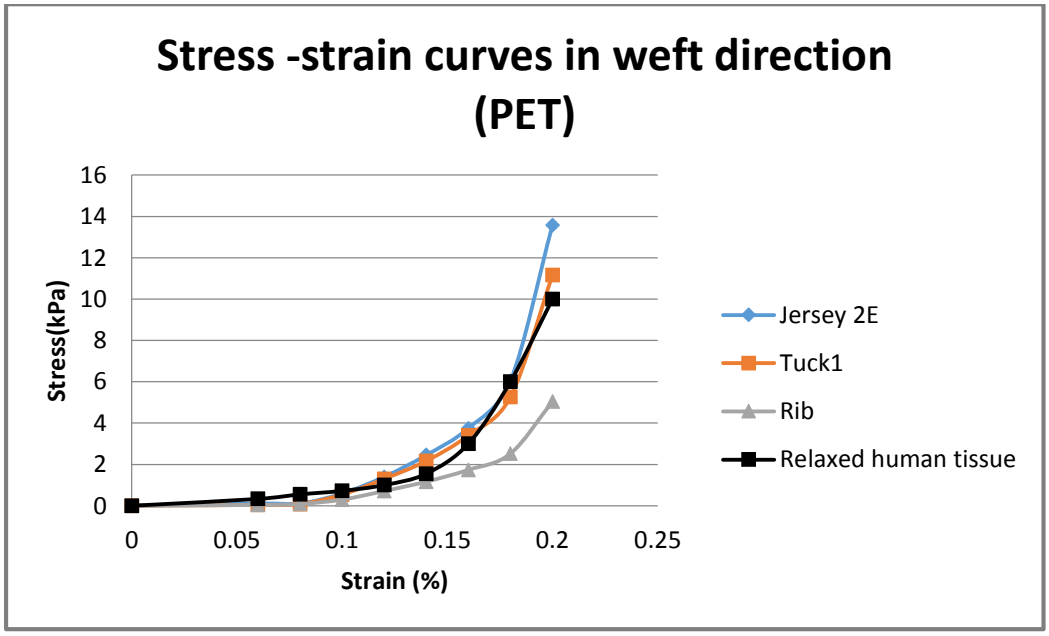

(b) Weft (horizontal) direction

Fig 4.5 Tensile stress-strain curves of PET jersey, tuck and rib stitch structures

These three prototype stitch structures were selected for the following reasons. For rib stitch, it had a modulus lower than the natural tissue in both directions. The percentage strain of this knitted structure was high, and the tensile stress-strain curve was close to that of human tissue. The porosity of the rib stitch structure was the highest among all the knitted samples. On account of the low tensile strain of PLA yarn, this rib structure is expected to perform well when knitted from PLA yarns. When considering the tuck stitch, its tensile stress-strain curve and modulus provided the closest match to that of the natural tissue in both directions. In comparison, the jersey stitch was selected as one of the structures because it complements the other two structures. The Young's modulus of the jersey stitch was the highest while the value for total porosity was the lowest of all the prototype samples. In summary, the jersey, tuck and rib stitch structures were selected as the three structures to be knitted as PLA prototype scaffolds.

4.2 Physical Properties of PLA Samples

The three prototype samples were knitted by folding two ends of 4-ply 324 denier PLA yarn. The same test methods were followed as described previously for the PET prototype samples.

4.2.1 Porosity

Table 4.3 Total porosity of PLA samples

	Thickness (mm)	Mass per unit area (g/m^2)	Total porosity (%)	
			Mean	Std Deviation
Jersey	0.87	330.26	69.41	1.21
Tuck	1.18	343.63	75.73	1.10
Rib	1.09	354.94	77.50	2.06

Based on Table 4.3 and Fig 4.6, the total porosity of the PLA samples ranged from 69.4% (jersey) to 77.5% (rib) compared with the equivalent polyester prototypes (84.2% for jersey, 92.3% for rib). The porosity of the same knitted stitch structures decreased by 15%-17% when the PET yarn was replaced with the PLA yarn. The main factors causing this shift are likely to be due to the thermal setting process and the bulk characteristic of the yarn itself.

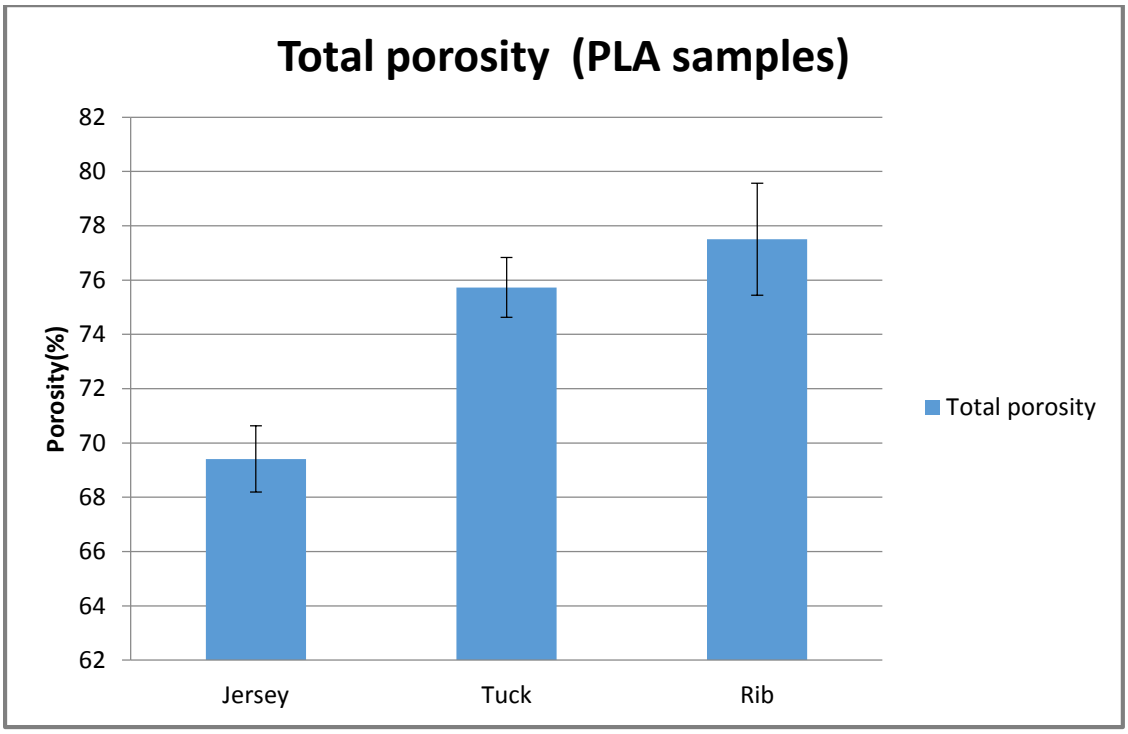

Fig 4.6 Total porosity of PLA samples

All the PLA samples were heat set for 5 min at 55 ℃ prior to biaxial mechanical and biological testing. During the heat setting process, the yarns and knitted structures shrank approximately 5% even though the edges of the fabrics were fixed with pins. The structures became tighter and lost porosity and their residual curl disappeared. As previously known, the rib stitch structures did not curl, but each PLA sample in this study was made under the same knitting and heat setting conditions. Another variable was the yarn itself. The diameter of the 4 ply PLA yarn was larger than the 2-ply PET yarn, which means that all the PLA fabrics had a consistently higher fabric density. Both factors contributed to the decrease in

total porosity, and the reduced porosity of the PLA fabrics posed a challenge for the proliferation of the CDC stem cells.

4.2.2 Results of Uniaxial Stretch and Recovery Test

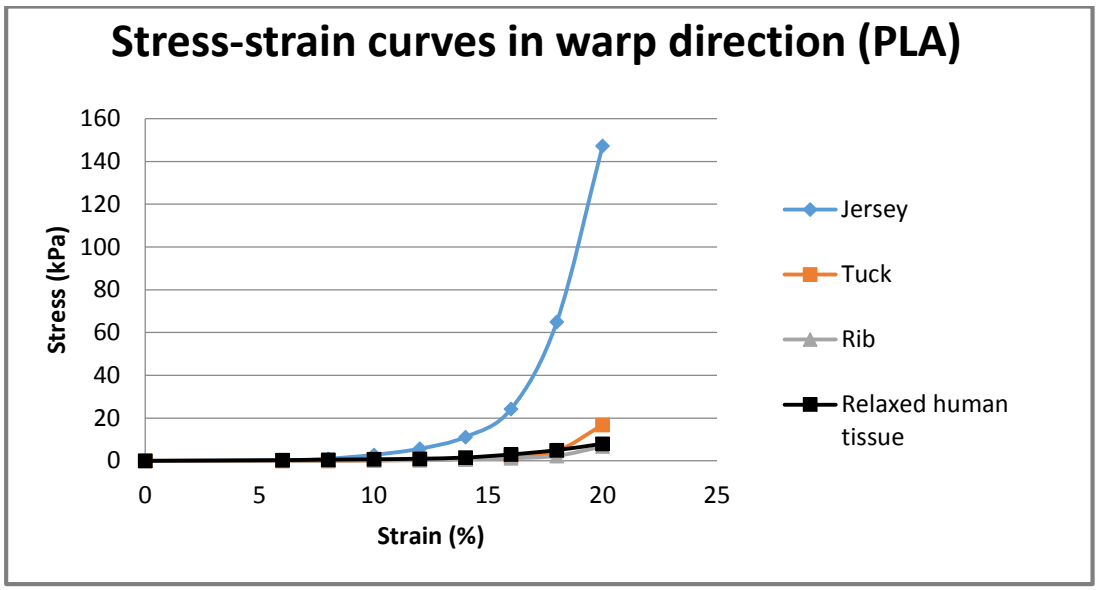

(a) Warp (vertical) direction

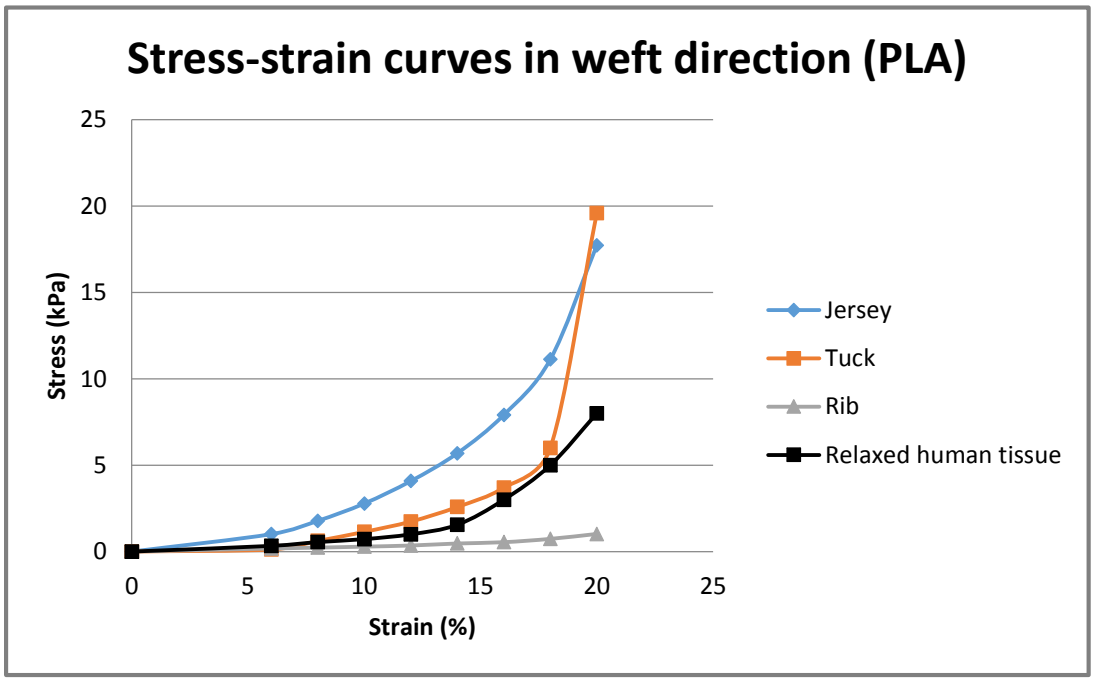

(b) Weft (horizontal) direction

Fig 4.7 Uniaxial tensile stress-strain curves of PLA samples

Based on Fig 4.7a the jersey stitch scaffold was associated with a significantly greater stiffness than the other scaffolds in the warp (vertical) direction. This means that the scaffold generated a much higher stress compared to the other samples at the same strain. As explained in Section 4.1.2, the percent strain of the jersey stitch structure was relatively low. So when rigid PLA yarns were involved, much higher mechanical stresses were measured during the tensile testing of the PLA jersey stitch knitted fabric. The two remaining curves representing the tuck and rib stitch samples gave a closer match to that of myocardial host tissue. The same trend was observed in the weft (horizontal) direction with Fig 4.7b. The tensile stress-strain curve of the tuck stitch mimicked that of human tissue during the first 18% strain. During the remaining 2% strain, the stress increased dramatically and the peak stress rose to a similar value as the jersey stitch. The conclusion is that the last segment of strain is probably dominated by the more rigid PLA yarns. For the rib stitch, the stress-strain curve lay below the human tissue curve, similar to the PET sample, indicating that the rib stitch structure itself with its low tensile modulus provided the major contribution to fabric elongation.

Table 4.4 Young's modulus of PLA samples in uniaxial test

	Young's Modulus (kPa)			
	Mean		Standard Deviation	
	Warp (Vertical)	Weft (Horizontal)	Warp (Vertical)	Weft (Horizontal)
Jersey	650.0	111.2	66.5	8.3
Tuck	46.1	59.9	11.5	4.0
Rib	33.6	5.1	5.1	0.6
Relaxed human tissue	50.0	50.0	N/A	N/A

In Table 4.4 and Fig 4.8, the results are similar to those reported above for the Young's modulus of the polyester scaffolds. The modulus of the jersey stitch sample at 20% strain reached 650 kPa in the warp direction and 111 kPa in the weft direction, which is several times higher than that of human tissue. In contrast, the stiffness of the rib stitch was much lower than that of human tissue. The modulus of the tuck stitch sample was similar to that of human myocardium. And the results of the stretch and recovery test demonstrated that the tuck stitch was the most promising structure for mimicking the mechanical properties needed for a cardiac patch.

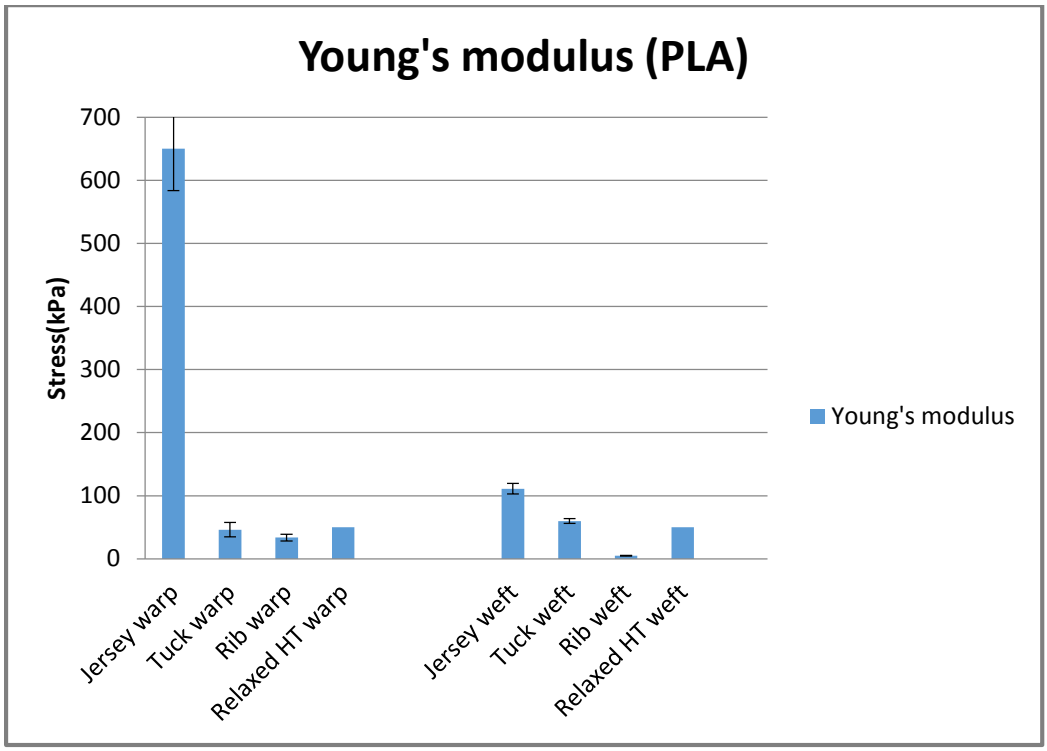

Fig 4.8 Uniaxial Young's modulus of PLA samples

4.2.3 Results of Biaxial Stretch and Recovery Test

Details about the morphological changes of weft (horizontal) knitted fabrics during mechanical testing have been described above They have involved measuring the tensile stress-strain curves in both directions with a uniaxial Instron mechanical tester. However in addition, a biaxial stretch and recovery test was undertaken to monitor the stress-strain performance in both directions simultaneously and observe the changes in the knit morphology over time. In order to accomplish this the PLA samples were cut into 1cm × 1cm square specimens and the central area of 6 mm×6mm was tested. For comparison

purposes rat myocardial tissue was selected as the control material, and the published mechanical properties of rat myocardium reported in Fujimoto's research paper are compared in Fig 4.9a, Fig 4.10a and Fig 4.11 with the mechanical performance of the PLA samples. (Fujimoto K L, 2007)

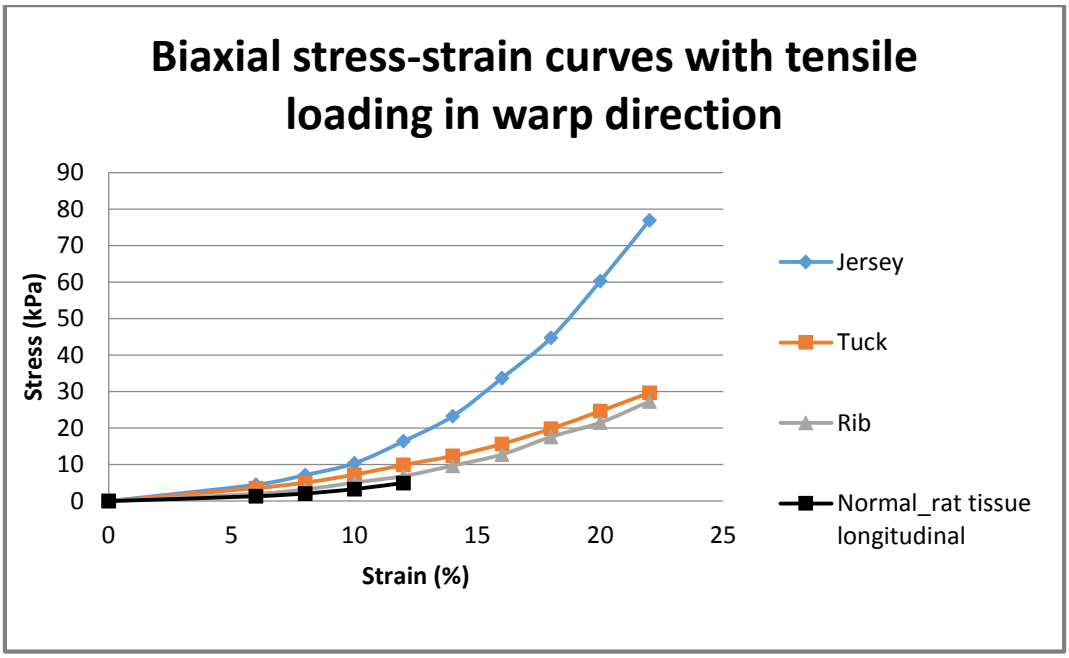

(a) Stress-strain curves measured in warp (vertical) direction

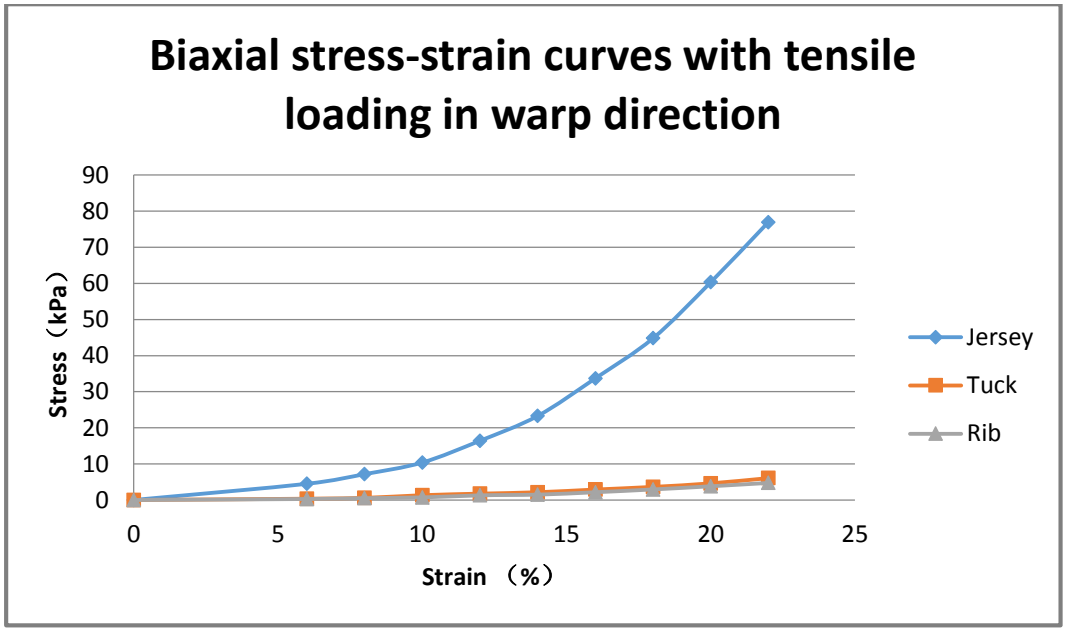

(b) Stress-strain curves measured in fixed weft (horizontal) direction

Fig 4.9 Results of biaxial test for PLA samples when stressed in the warp (vertical) direction

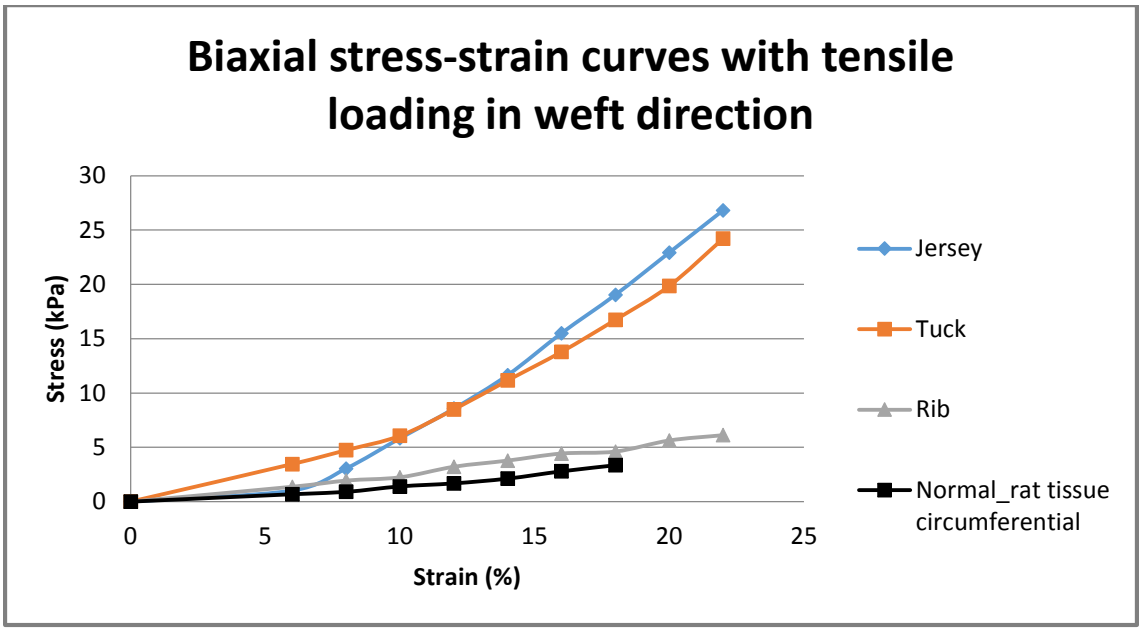

(a) Stress-strain curves measured in weft (horizontal) direction

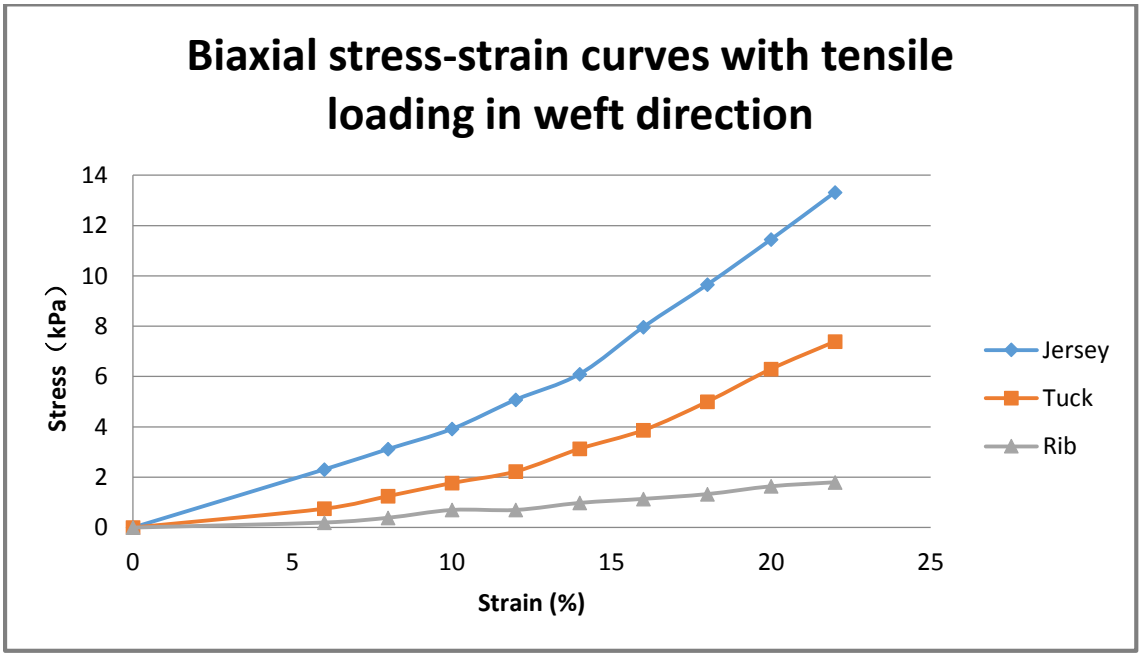

(b) Stress-strain curves measured in fixed warp (vertical) direction

Fig 4.10 Result of biaxial test for PLA samples when stressed in the weft (horizontal) direction

As a result of the biaxial tests with the applied tensile load in the warp direction (Fig 4.9a), the stress-strain curves of the jersey and tuck stitches in the warp direction are similar to each other and are above the curve for the rat tissue. When the tensile load is applied in the weft direction (Fig 4.10a), the jersey stitch data and the tuck stitch results follow similar curves in the weft direction, similar to the trend observed during uniaxial Instron testing. It is of interest to note that the mechanical properties of rat tissue almost match those of the rib stitch samples in both directions. In fact the rib stitch scaffold imitates closely the mechanical performance of the rat tissue in this particular biaxial test.

When either the warp or weft direction was stretched during the biaxial test, the other (or cross) direction was held in a fixed condition. The loops of knitted yarns in the test direction tended to move closer together once the fabric structure failed to offer any further elongation, which led to some shrinkage in the fixed cross direction. The presence of high stresses in the cross direction may cause changes in the scaffolds shape and morphology during implantation due to relative movement between the scaffold and the pericardial tissue. In fact these high stresses are likely to influence the attachment of the scaffold, the stability of its structure and its mechanical performance adjacent to the heart tissue. As seen in Fig 4.9b and Fig 4.10b, the force in the fixed cross direction for the jersey and tuck stitches is higher than that for the rib stitch structure. As the result, according to these biaxial test results, the rib structure appears to provide the best structural stability of all the PLA scaffolds.

During the analysis of these results so far, the mechanical properties in the warp direction have been compared with the longitudinal direction of the pericardial tissue, and the weft direction of the knitted scaffold has been compared with the circumferential direction of the

heart. However, in Fig 4.11, the orientation of the knitted structure has been turned through 90 degrees so as to make the warp direction of the scaffold correspond with the circumferential direction of the myocardium and vice versa.

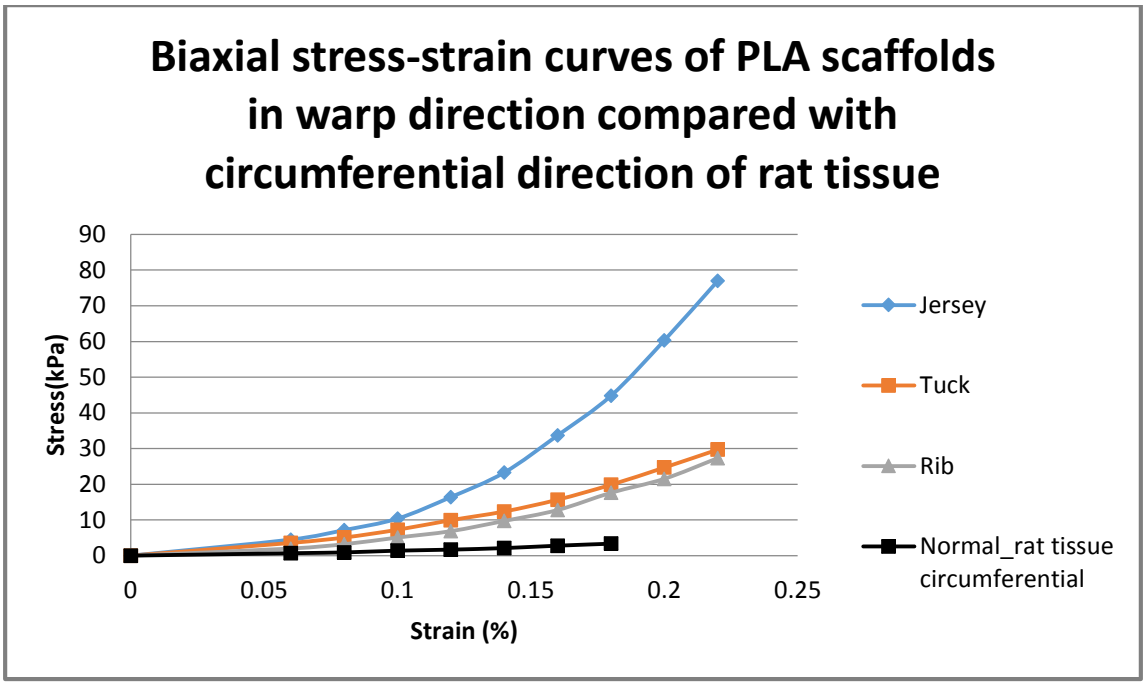

(a)

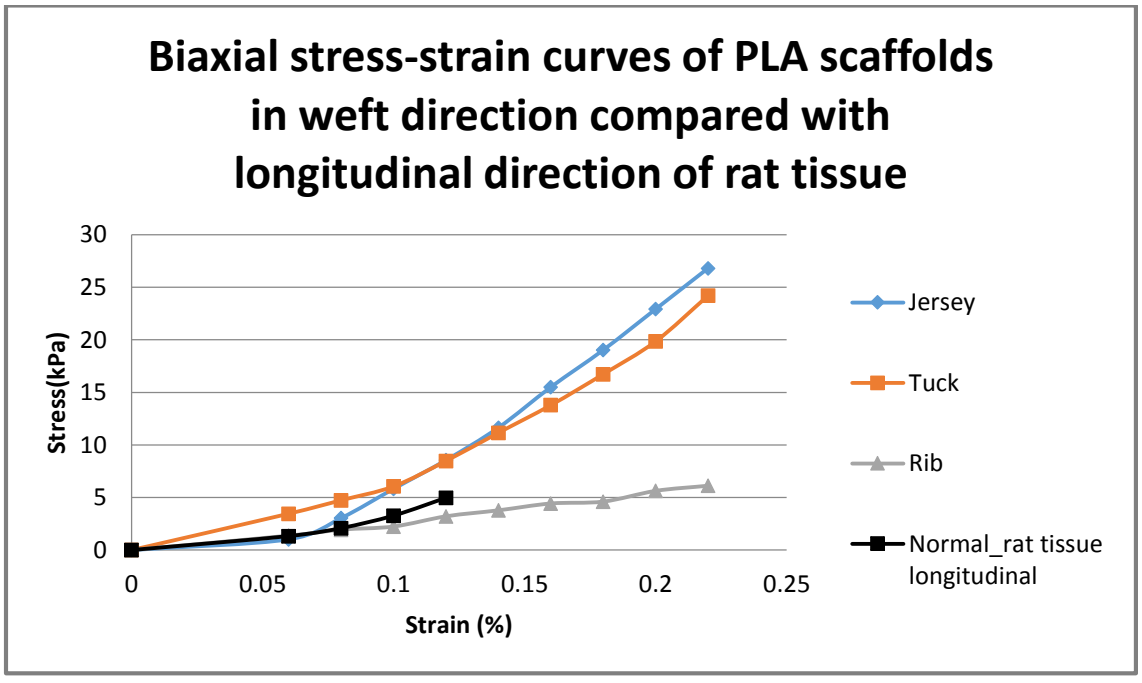

(b)

Fig 4.11 Results of biaxial test for PLA samples after changing orientation though 90 degrees

As shown in Fig 4.11, none of the three weft knitted stitch structures provides a close match to the mechanical properties of rat tissue when the PLA scaffold's orientation has been changed through 90 degrees. So it is worth noting that the preferred orientation for implanting the scaffold is to align the PLA scaffold's warp direction parallel to the longitudinal direction of the myocardial tissue. This gives a much closer mechanical match than when the orientation of the scaffold has been rotated through 90 degrees.

Table 4.5 Young's modulus of PLA samples in biaxial test

	Young's modulus (kPa)			
	Mean		Standard Deviation	
	Warp (Vertical / Longitudinal)	Weft (Horizontal / Circumferential)	Warp (Vertical / Longitudinal)	Weft (Horizontal / Circumferential)
Jersey	301.5	114.7	52.7	13.0
Tuck	123.2	99.3	29.0	13.0
Rib	107.7	28.2	10.1	7.1
Normal_rat tissue	41.5	18.6	N/A	N/A

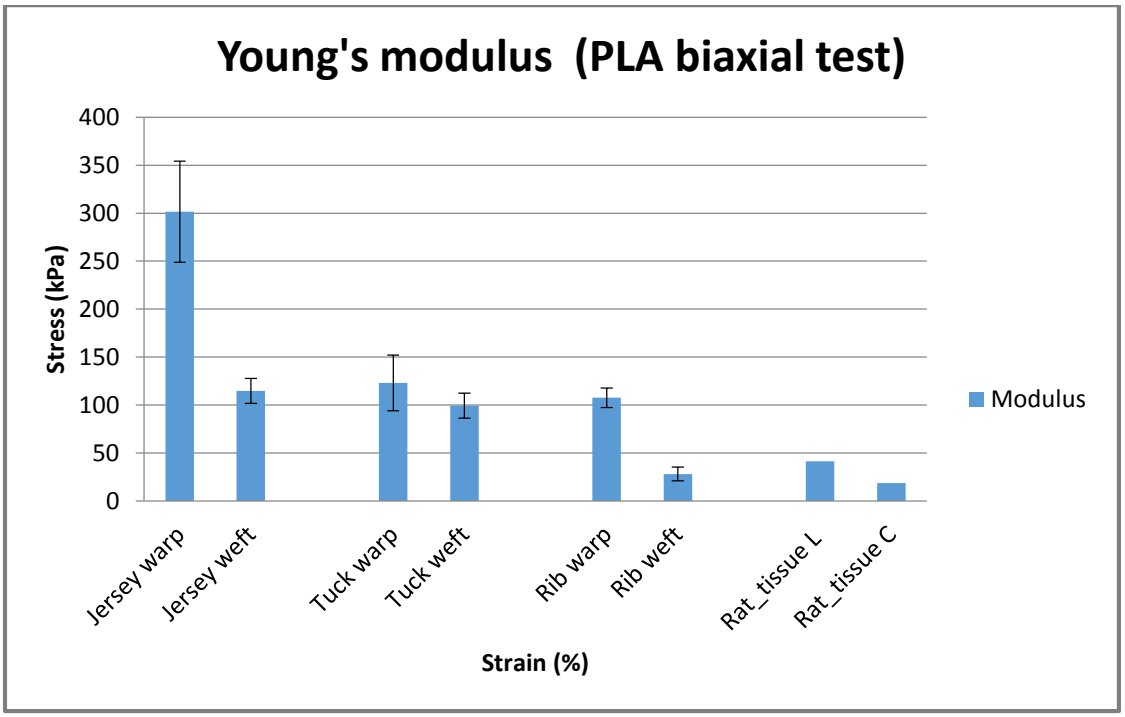

Fig 4.12 Young's modulus of PLA samples in biaxial test

By analyzing Table 4.5 and Fig 4.12, one can conclude that the rib stitch structure had a Young's modulus that was the closest match to rat myocardial tissue. The rib stitch gave the best performance of the three PLA samples when tested by the biaxial test procedure. Based on these mechanical test results, both the tuck and the rib stitch structures are promising candidates for fabricating a mechano-compatible cardiac patch. The final selection will depend on the size of the patch, the animal model under investigation as well as other factors.

4.3 Biological Performance

4.3.1 Cell Viability and Proliferation by MTT Assay

Table 4.6 Results of MTT assay

		Jersey	Tuck	Rib	Control
Mean	Day 0	0.200	0.160	0.140	0.140
Std Dev	Day 0	0.035	0.023	0.014	0.014
Mean	Day 7	0.310	0.320	0.450	0.570
Std Dev	Day 7	0.033	0.066	0.070	0.110

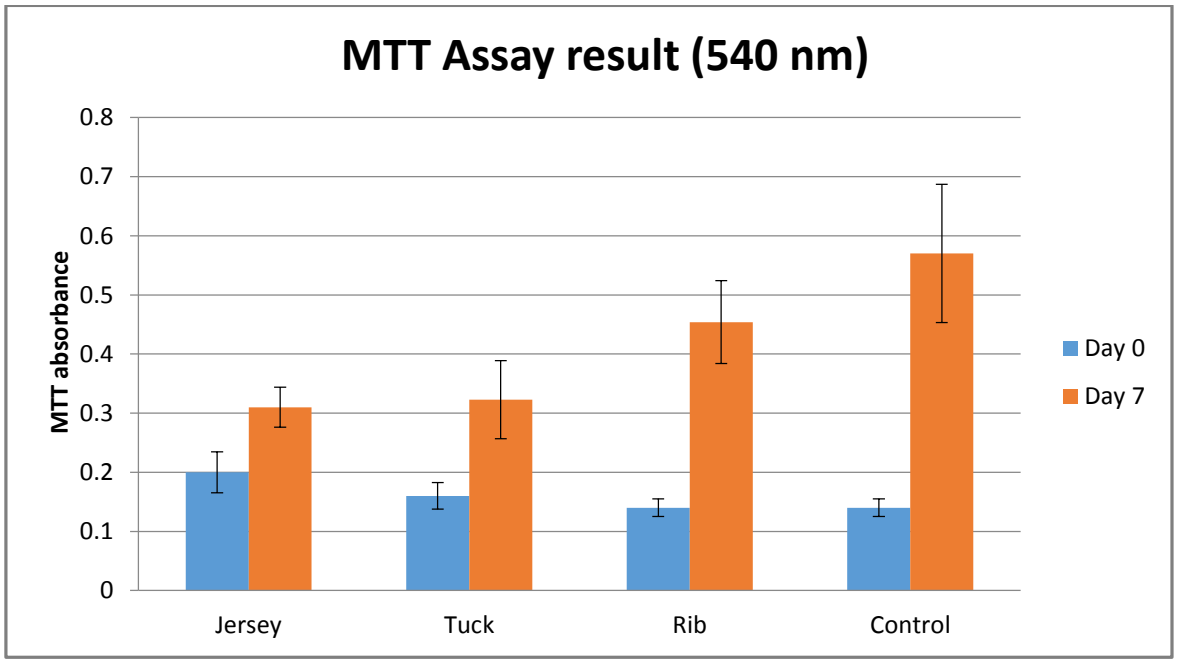

Fig 4.13 Results of MTT assay

The use of an MTT assay is a routine method to measure cell viability and the extent of cell proliferation on tissue engineering scaffolds. By finding sufficient cell viability and proliferation one can confirm the biocompatibility of the scaffold. As mentioned in Chapter 3 the MTT assay was conducted on Day 0 and Day 7. The mean values and standard deviations for the absorbance measurements are listed in Table 4.6. Fig 4.13 displays the differences between the scaffolds and the control group.

For each type of scaffold, the result at Day 7 was significantly higher than at Day 0 ($p<0.05$). This suggests that the cells successfully attached and proliferated on the scaffolds. However, the absorbance for the three PLA samples was lower than for the control group. This would have been caused by differences in surface area. Compared with the rib stitch scaffold, the absorbance by both the jersey and tuck stitch samples was significantly lower. This may have been attributed to the lower porosity of the jersey and tuck scaffolds ($p<0.05$). The rib stitch structure had the highest porosity, highest density and lowest Young's modulus of the three PLA scaffolds, which means that there was more space between the yarns and more yarns per unit area to promote cell attachment and infiltration. More space between yarns generates more channels for the delivery of nutrients and oxygen to living cells and the removal of metabolites. In addition, more yarns means that there is a larger surface area for cell attachment and proliferation. Therefore, the rib stitch structure is the most suitable structure for cell proliferation.

4.3.2 Cell Attachment by SEM

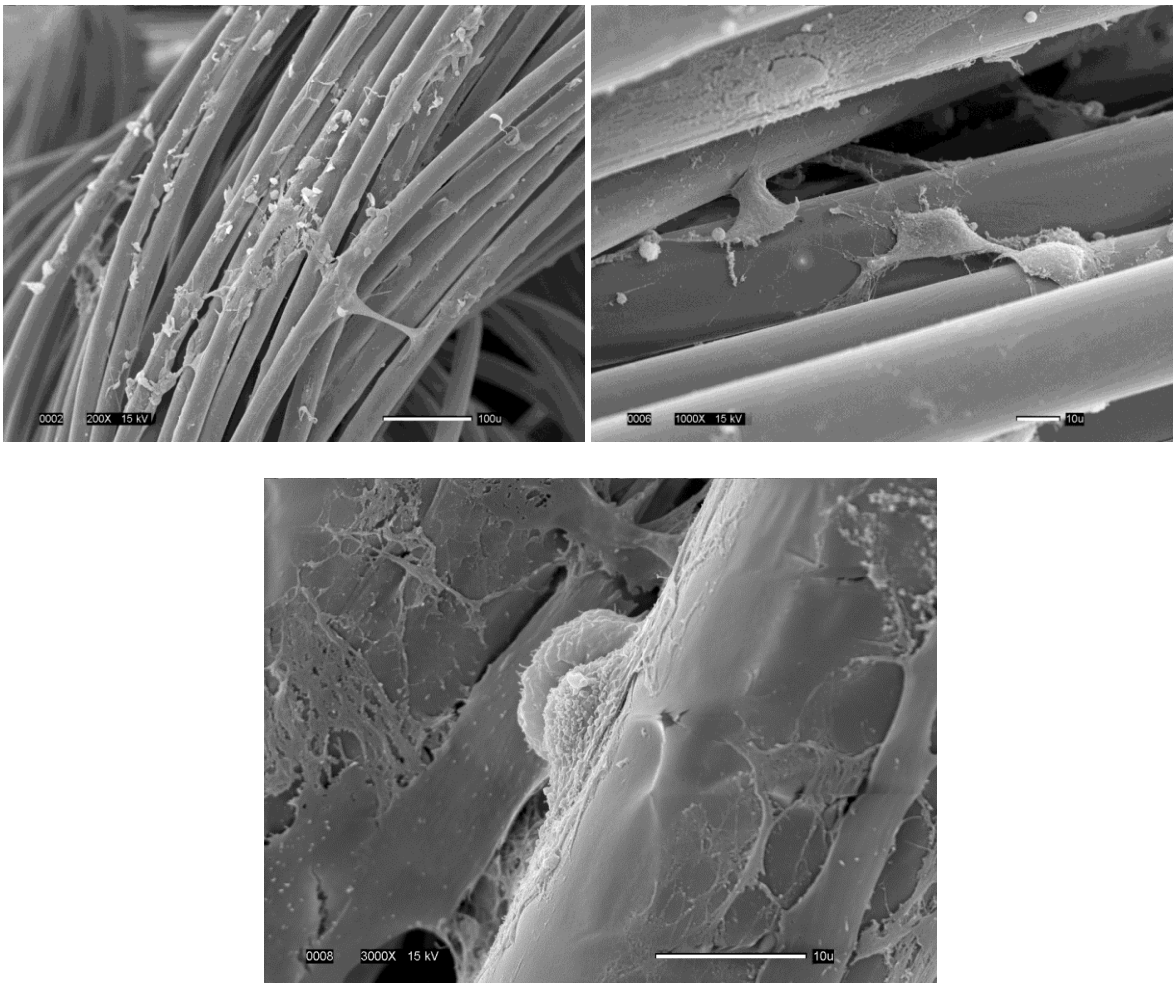

Fig 4.14 SEM images of CDCs attached to PLA fibers

(a) 200X, (b) 1000X, (c) 3000X magnification

While the proliferation of the CDCs on PLA yarns has been quantified by the MTT assay, cell attachment and morphology has been confirmed by scanning electron microscopy (SEM). In Fig 4.14 the cells are seen attaching themselves and growing along the surface of the PLA

fibers. Over longer periods of culture the cells will reach confluence, and the next step in their evaluation will involve implantation in animal models and clinical trials.

The above images show that CDCs cells can become well attached to the surface of the PLA fibers. There is also evidence to demonstrate that the cells can differentiate and migrate along the surface of the yarns and between the PLA fibers. In the future, the gene expression and phenotype of the living cells will be determined by a range of different markers and techniques such as the Green Fluorescent Protein (GFP) test for use with an animal model.

CHAPTER 5

CONCLUSIONS AND FUTURE WORK

5.1 Conclusions

A PLA knitted cardiac patch for seeding CDCs was designed and knitted as described in Chapter 3. The results of mechanical and biological testing has been presented, discussed and analyzed in Chapter 4. Based on these results, the goals of the study were achieved as follows.

1. Both polyester and polyester/spandex patches were successfully knitted on a Shima Seiki weft knitting machine. The rib stitch structure had the highest porosity among all the samples while the jersey 2E had the lowest porosity.
2. Based on the results of the stretch and recovery tests, most of the samples mimicked the stress-strain curve of human myocardium. The applied tensile stress and Young's modulus at 20% strain experienced by the rib stitch structure were the lowest of all the different stitch structures tested. On the other hand, the jersey 2E polyester sample had the highest stiffness among all the samples. The reduction in Young's modulus with the introduction of the spandex yarns was not significant ($p>0.05$). Moreover, the mechanical properties of the rib and tuck stitch polyester samples were ideal alternative structures to replace the spandex blended samples since they were not biodegradable. Jersey, tuck and rib stitch knits were selected as the structures for further fabrication and testing with PLA yarns
3. The mechanical properties of the PLA samples were close to those of the polyester

samples. In the uniaxial Instron tensile test, the jersey sample was stiffer than relaxed myocardial human tissue, while the rib stitch sample was weaker than the natural tissue control. The tuck stitch sample mimicked most closely the mechanical properties of the pericardial tissue. In the biaxial stretch and recovery test, both jersey and tuck stitch samples had a higher Young's modulus than rat myocardium, and the rib sample closely simulated the mechanical properties of rat myocardium. As a result, both tuck and rib stitch structures appear to be the most promising candidates for knitting cardiac patches.

4. The attachment and growth of CDCs was observed by SEM. The cells were able to attach themselves to the surface of the PLA fibers and migrate along or between the fibers. SEM observations showed good biocompatibility between the PLA yarns and the CDCs, which means that the PLA cardiac patch has the potential to be successful if applied in an animal model and/or clinical trial.
5. The proliferation of CDCs on the rib stitch scaffold was significantly greater than that on the jersey and tuck scaffolds. This may be attributed to the high porosity and mass per unit area of the rib stitch scaffold. Based on these results, the rib stitch structure provided the optimum scaffold for the seeding and proliferation of CDCs in this study.

After successfully achieving the above five objectives, the conclusion of this study is that the rib stitch structure is the most promising structure for use as a cardiac patch. The superior elasticity of the rib scaffold will not restrict the cardiac diastole and at the same time will provide a certain level of support for the myocardium. The results from the biocompatibility and cell proliferation assays demonstrate that the rib stitch scaffold has the potential to deliver CDCs directly to the injured site and regenerate the myocardium.

5.2 Future Work

From the above conclusions, it is now feasible to propose the following additional changes that would improve further the mechanical and biological performance of the weft knitted cardiac patches described in this study.

1. From the point of view of fabrication and treatment, the parameters of knitting a rib stitch fabric can be improved to increase the stiffness of the rib stitch fabric, which is currently marginally lower than the host tissue. For example, the gauge could be decreased to make the fabric tighter and increase the modulus of the rib structure. The parameters should be optimized so as to balance both the Young's modulus and the total porosity.
2. The material selection for the cardiac patch can also be improved. In this study, PLA was chosen as the raw material to knit cardiac patches because PLA has been approved by the FDA to be used to generate various kinds of implantable medical devices. In actual fact, PLA has already been combined with a variety of other synthetic and natural polymers to achieve different properties such as PLA/collagen fibers, a PLA/PEG poly(ethylene glycol) copolymer and a PLA/fibroin composite.

   Except PLA, Murthy et al have developed a resorbable polymer based on poly-ketal chemistry which has the advantage of degrading into neutral by-products with no acidic species. It could be a promising material for generating a cardiac patch for the delivery of stem cells.
3. All these materials have been used to build different tissue engineering scaffolds for the regeneration of various tissues. They could point us in a promising direction to further improve the properties of weft knitted cardiac patches.

4. In order to determine the in vivo function of this type of cardiac patch, an animal trial needs to be designed for future research. It is recommended that knitted heart patches be implanted in a small animal model such as the rat, and the survival rate of the cells, the cardiac ejection fraction, the scar tissue size and thickness of the ventricular wall should be measured to determine the in vivo function of the cardiac patch.
5. The question of how a cardiac patch might be attached to a patient's myocardial tissue still remains unanswered. It is suggested that the direction for future research could consider a type of tissue adhesive that would be applied to the cardiac patch during an animal trial. The glue would fix the cardiac patch to the myocardium and a novel delivery system needs to be designed for minimally invasive surgery in the future.

REFERENCES

Arnal-Pastor, M., Chachques, J. C., Pradas, M. M., & Vallés-Lluch, A. (2013). Biomaterial for Cardiac Tissue Engineering. In Regenerative Medicine and Tissue Engineering (p. 275). Valencia: Intech.

Asiri, A. M., Marwani, H. M., Khan, S. B., & Webster, T. J. (2014). Greater cardiomyocyte density on aligned compared with random carbon nanofibers in polymer composites. International Journal of Nanomedicine, 9, 5533.

Berk, B. C., Fujiwara, K., & Lehoux, S. (2007). ECM remodeling in hypertensive heart disease. Journal of Clinical Investigation, 117(3), 568.

Boilson, B. A., Raichlin, E., Park, S. J., & Kushwaha, S. S. (2010). Device therapy and cardiac transplantation for end-stage heart failure. Current Problems in Cardiology, 35(1), 8-64.

Boublik, J., Park, H., Radisic, M., Tognana, E., Chen, F., Pei, M., ... & Freed, L. E. (2005). Mechanical properties and remodeling of hybrid cardiac constructs made from heart cells, fibrin, and biodegradable, elastomeric knitted fabric. Tissue Engineering, 11(7-8), 1122-1132.

Burkhoff, D., Klotz, S., & Mancini, D. M. (2006). LVAD-induced reverse remodeling: basic and clinical implications for myocardial recovery. Journal of Cardiac Failure, 12(3), 227-239.

Burke AP, Virmani R. Pathology of myocardial ishchemia, infarction, reperfusion and sudden death. In: Fuster V,Walsh RA, O'Rourke TA, Poole-Wilson P(ed.) Hurst's the Heart. 12th Edition, McGraw-Hill Professional; 2010. p1321-1338

Chen, Q. Z., Bismarck, A., Hansen, U., Junaid, S., Tran, M. Q., Harding, S. E., ... & Boccaccini, A. R. (2008). Characterisation of a soft elastomer poly(glycerol sebacate) designed to match the mechanical properties of myocardial tissue. Biomaterials, 29(1), 47-57.

Chen, Y., Wang, J., Shen, B., Chan, C. W., Wang, C., Zhao, Y,. & Wu, H. (2015). Engineering a freestanding biomimetic cardiac patch using biodegradable poly(lactic-co-glycolic acid) (PLGA) and human embryonic stem cell-derived ventricular cardiomyocytes (hESC‐VCMs). Macromolecular Bioscience, 15(3), 426-436.

Cheng, K., Malliaras, K., Shen, D., Tseliou, E., Ionta, V., Smith, J., ... & Marbán, E. (2012). Intramyocardial injection of platelet gel promotes endogenous repair and augments cardiac function in rats with myocardial infarction. Journal of the American College of Cardiology, 59(3), 256-264

Dabiryan, H., Jeddi, A. A., & Rastgoo, A. (2013). Analysis of warp knitted fabric structure. Part V: experimental study on the initial modulus of warp knitted fabrics. Journal of the Textile Institute, 104(1), 46-56.

Di Bella, C., Farlie, P., & Penington, A. J. (2008). Bone regeneration in a rabbit critical-sized skull defect using autologous adipose-derived cells. Tissue Engineering Part A, 14(4), 483-490.

Dvir, T., Timko, B. P., Brigham, M. D., Naik, S. R., Karajanagi, S. S., Levy, O., ... & Kohane, D. S. (2011). Nanowired three-dimensional cardiac patches. Nature Nanotechnology, 6(11), 720-725.

Fujimoto, K. L., Guan, J., Oshima, H., Sakai, T., & Wagner, W. R-. (2007). In vivo evaluation of a porous, elastic, biodegradable patch for reconstructive cardiac procedures. Annals of Thoracic Surgery, 83(2), 648-654.

Garlotta, D. (2001). A literature review of poly(lactic acid). Journal of Polymers and the Environment, 9(2), 63-84.

Go, A. S., Mozaffarian, D., Roger, V. L., Benjamin, E. J., Berry, J. D., Blaha, M. J. & Stroke, S. S. (2014). Heart disease and stroke statistics--2014 update: a report from the American Heart Association. Circulation, 129(3), e28.

Guidoin, R. G., King, M., Marois, M., Martin, L., Marceau, D., Hood, R., & Maini, R. (1986). New polyester arterial prostheses from Great Britain: an in vitro and in vivo evaluation. Annals of Biomedical Engineering, 14(4), 351-367.

Hofmann M, Wollert KC, Meyer GP, Menke A, Arseniev L, Hertenstein B, Ganser A, Knapp WH, Drexler H. Monitoring of bone marrow cell homing into the infarcted human myocardium. Circulation 2005; 111: 2198-202.

Johnston, P. V., Sasano, T., Mills, K., Evers, R., Lee, S. T., Smith, R. R., ... & Marbán, E. (2009). Engraftment, differentiation, and functional benefits of autologous cardiosphere-derived cells in porcine ischemic cardiomyopathy. Circulation, 120(12), 1075-1083.

Kochupura, P. V., Azeloglu, E. U., Kelly, D. J., Doronin, S. V., Badylak, S. F., Krukenkamp, I. B., & Gaudette, G. R. (2005). Tissue-engineered myocardial patch derived from extracellular matrix provides regional mechanical function. Circulation, 112(9 suppl), I-144.

Konstam, M. A., Kramer, D. G., Patel, A. R., Maron, M. S. & Udelson, J. E. (2011). Left ventricular remodeling in heart failure: current concepts in clinical significance and assessment. JACC: Cardiovascular Imaging, 4(1), 98-108.

Laflamme, M. A., & Murry, C. E. (2005). Regenerating the heart. Nature Biotechnology, 23(7), 845-856.

Li, T. S., Cheng, K., Malliaras, K., Smith, R. R., Zhang, Y., Sun, B., ... & Marbán, E. (2012). Direct comparison of different stem cell types and subpopulations reveals superior paracrine potency and myocardial repair efficacy with cardiosphere-derived cells. Journal of the American College of Cardiology, 59(10), 942-953.

Lindner, D., Zietsch, C., Tank, J., Sossalla, S., Fluschnik, N., Hinrichs, S., ... & Westermann, D. (2014). Cardiac fibroblasts support cardiac inflammation in heart failure. Basic Research in Cardiology, 109(5), 1-16.

Lopes, M. S., Jardini, A. L., & Maciel Filho, R. (2012). Poly(lactic acid) production for tissue engineering applications. Procedia Engineering, 42, 1402-1413.

Lu, X., (2014). Multiple layer nerve guide for peripheral nerve regeneration using carbon nanotubes. MS thesis, North Carolina State University, Raleigh, USA

Mankad, A. K., Tang, D. G., Clark, W. B., Flattery, M., Harton, S., Katlaps, G. J., ... & Shah, K. B. (2012). Persistent anemia after implantation of the total artificial heart. Journal of Cardiac Failure, 18(6), 433-438.

Makkar, R. R., Smith, R. R., Cheng, K. E., Malliaras, K., Thomson, L. E., Berman, D., & Marbán, E. (2012). Intracoronary cardiosphere-derived cells for heart regeneration after myocardial infarction (CADUCEUS): a prospective, randomised phase 1 trial. The Lancet, 379(9819), 895-904.

Mann, D. L. (1999). Mechanisms and models in heart failure a combinatorial approach. Circulation, 100(9), 999-1008.

Mirensky, T., & Breuer, C. K. (2008). The development of tissue engineered grafts for reconstructive cardiothoracic surgical applications. Pediatric Research, 63, 559–568

Miyagi, Y., Chiu, L. L., Cimini, M., Weisel, R. D., Radisic, M., & Li, R. K. (2011). Biodegradable collagen patch with covalently immobilized VEGF for myocardial repair. Biomaterials, 32(5), 1280-1290.

Nian, M., Lee, P., Khaper, N., & Liu, P. (2004). Inflammatory cytokines and postmyocardial infarction remodeling. Circulation Research, 94(12), 1543-1553.

Ozawa, T., Mickle, D. A., Weisel, R. D., Koyama, N., Ozawa, S., & Li, R. K. (2002). Optimal biomaterial for creation of autologous cardiac grafts. Circulation, 106(12 suppl 1), I-176.

Pok, S., & Jacot, J. G. (2011). Biomaterials advances in patches for congenital heart defect repair. Journal of Cardiovascular Translational Research, 4(5), 646-654.

Prabhakaran, M. P., Kai, D., Ghasemi-Mobarakeh, L., & Ramakrishna, S. (2011). Electrospun biocomposite nanofibrous patch for cardiac tissue engineering. Biomedical Materials, 6(5), 055001.

Radisic, M., Fast, V. G., Sharifov, O. F., Iyer, R. K., Park, H., & Vunjak-Novakovic, G. (2008). Optical mapping of impulse propagation in engineered cardiac tissue. Tissue Engineering Part A, 15(4), 851-860.

Raman, J. (2008). Management of Heart Failure: Volume 2: Surgical (Vol. 2).11-13 Springer Science & Business Media.

Ratner, B. (2013). Chapter 1.2.2 Polymers：basic principles. In Biomaterials Science an Introduction to Materials in Medicine (3rd Ed., pp. 70-80). Waltham, MA: Academic Press.

Ray, S. C. (2012). Fundamentals and Advances in Knitting Technology. Woodhead Publishing Limited, Cambridge, UK

ScienCell (2015) MTT assay protocol. Retrieved from https://sciencellonline.com/downloads/dl/file/id/36/8028.pdf

Segers, V. F., & Lee, R. T. (2008). Stem-cell therapy for cardiac disease. Nature, 451(7181), 937-942.

Smith, R. R., Barile, L., Cho, H. C., Leppo, M. K., Hare, J. M., Messina, E., ... & Marbán, E. (2007). Regenerative potential of cardiosphere-derived cells expanded from percutaneous endomyocardial biopsy specimens. Circulation,115(7), 896-908.

Sun, Y., Kiani, M. F., Postlethwaite, A. E., & Weber, K. T. (2002). Infarct scar as living tissue. Basic Research in Cardiology, 97(5), 343-347.

Srinivasan, A., & Sehgal, P. K. (2009). Characterization of biocompatible collagen fibers—a promising candidate for cardiac patch. Tissue Engineering Part C: Methods, 16(5), 895-903.

Wang F, Guan J. Cellular cardiomyoplasty and cardiac tissue engineering for myocardial Therapy. Advanced Drug Delivery Reviews 2010; 62: 784–797.

Wu, X. (2012). Surface modification of polylactic acid nonwoven webs. MS thesis, North Carolina State University, Raleigh, USA

Vunjak-Novakovic, G., Tandon, N., Godier, A., Maidhof, R., Marsano, A., Martens, T. P., & Radisic, M. (2009). Challenges in cardiac tissue engineering. Tissue Engineering Part B: Reviews, 16(2), 169-187.